

Bipartite entanglement via distance between the states in a one dimensional spin 1/2 dimer copper acetate monohydrate

S. Athira,¹ Saulo L. L. Silva,² Sushma Lakshmi,¹ Sharath Kumar C,¹
Debendra Prasad Panda,³ Sayan Das,⁴ Probal Nag,⁴ Andrews P. Alex,¹ A.
Sundaresan,³ Sivaranjana Reddy Vennapusa,⁴ and D. Jaiswal-Nagar^{1,*}

¹*School of Physics, IISER Thiruvananthapuram,*

Vithura, Thiruvananthapuram-695551, India

²*Centro Federal de Educação Tecnológica,*

CEFET-MG, Nepomuceno-37250000, Brazil

³*School of Advanced Materials, and Chemistry and Physics of Materials Unit,
Jawaharlal Nehru Centre for Advanced Scientific Research, Jakkur, Bangalore-560064, India*

⁴*School of Chemistry, IISER Thiruvananthapuram,*

Vithura, Thiruvananthapuram-695551, India

(Dated: March 10, 2023)

arXiv:2303.05372v1 [cond-mat.str-el] 9 Mar 2023

Abstract

In this paper, we used a theoretical measure known as distance between the states, $\mathcal{E}(\rho_e)$, to determine the bipartite entanglement of a one dimensional magnetic dimer system. The calculation was compared with the well-known entanglement measure, concurrence, and found to be the same. $\mathcal{E}(\rho_e)$ was, then, expressed in terms of two thermodynamic quantities, namely, magnetic susceptibility and specific heat. Experimental verification of temperature variation of the bipartite entanglement measure in terms of magnetic susceptibility and specific heat was done on single crystals of copper acetate-an excellent one dimensional dimer system. The results showed the existence of bipartite entanglement till temperatures as high as room temperature! Large sized single crystals of copper acetate were grown by a new evaporation technique and characterised by TGA, IR and Raman spectroscopy measurements. Density functional theory calculations were done to calculate the delocalisation index which showed much lower values of $\delta(Cu, Cu)$ than other bonds, implying that the probability of direct Cu-Cu exchange in copper acetate is very small.

I. INTRODUCTION

Low dimensional magnets have been at the forefront of research recently due to pronounced quantum effects seen in them at finite temperatures as a consequence of low dimensions [5]. The quantum effects are expected to be more pronounced when the total spin quantum number S of the low dimensional magnet is small: smaller the spin quantum number, higher the quantum fluctuations[2]. So, a one dimensional quantum magnet with $S = 1/2$ is expected to show the most pronounced quantum mechanical effects since the spatial dimensionality is the lowest at 1 and the spin quantum number S is lowest at $1/2$. Therefore, spin $1/2$ ions such as Cu(II) have been extensively used to study low dimensional quantum molecular magnetism. In recent times, low dimensional magnets have also been studied extensively in the area of quantum information processing where the $S = 1/2$ spin chains are treated as a bus that link quantum information processors [16–18]. Here, entanglement between spins results in superposition states of spins being held for a long time and consequently, entanglement being used as a resource. Entanglement exemplified as a superposition

* deepshikha@iisertvm.ac.in

of two spin 1/2 states, $(1/\sqrt{2})(|\uparrow\downarrow\rangle - |\downarrow\uparrow\rangle)$ is one of the most intriguing quantum mechanical phenomena where a coherent superposition of states cannot be written as product states of individual wavefunctions [19–24]. Using such entangled states, quantum protocols such as teleportation [26, 29, 30], can be realised for perfect transportation of quantum states. There exist various measures to quantify entanglement [16, 19, 20, 23, 24, 31, 34–37, 40], however, no unique measure of entanglement is expected even for mixed bipartite states [20, 24, 35].

Spin dimer Heisenberg antiferromagnetic chain (HAfc) systems are those systems in which the nearest neighbour spins interact with each other via two exchange coupling constants J_1 and J_2 such that $J_2 \ll J_1$ resulting in pair of spins being alternately coupled by strong and weak bonds governed by two different values of exchange coupling constants [13, 41, 67]. The ground state of a dimer HAfc system is non-magnetic comprising spin singlets and is separated from a triplet excited state (consisting of triplons) by a finite spin gap Δ . When J_1 is not appreciably different from J_2 , the dimeric chain is called an alternating chain defined with an alteration parameter $\alpha = J_2/J_1$, such that $0 < \alpha < 1$. The alternate chain systems with variable values of α have been in intense limelight recently due to their relevance in quantum information theory, wherein, they have been used as a model system in studying bipartite entanglement measures like concurrence [20, 21, 42].

A finite interdimer interaction converts the dimer system to an alternating chain material affecting the value of the energy gap Δ . In order for a spin dimer to be used as an information storage or a quantum computing material, it should mimic the idealised dimer system as closely as possible. The various reported spin dimer systems have a value of α that is small but in the range of 0.1-0.3 [1, 6, 11–13, 25]. However, the celebrated dimer system tetrakis(acetate) diaquadicopper ($C_8H_{16}Cu_2O_{10}$)-copper acetate for short [48] has a very small value of the alteration parameter α and represents the model system on which entanglement measures for a dimer system could be tested. In this paper, we employ a bipartite measure of entanglement, namely, "distance between the states" for a magnetic dimer system in terms of which two thermodynamic quantities, namely, magnetic susceptibility and specific heat is expressed. The equivalence of this measure to a well-known measure, namely, concurrence is also shown. The calculations are tested on copper acetate-the celebrated one dimensional dimer system, that was grown using a new synthesis method resulting in large-sized single crystals. The structure of copper acetate was confirmed with single crystal x-ray

diffraction. Fourier transform infrared spectroscopy and Raman spectroscopy was done to identify the prominent relevant bands in the structure that were confirmed by density functional theory calculations employing a mixed basis having a metal centre and an organic part [43, 44]. Further, delocalisation index was calculated for different bonds and it was found that the delocalisation index value for direct Cu-Cu bonds was much lower than other bonds implying that the probability of direct Cu-Cu exchange in copper acetate is quite small.

II. THEORY

A. Bipartite Entanglement measure: Distance between the states

Vedral et al. [47] proposed a new measure of entanglement, namely, distance between the states, \mathcal{D} , in the quantum mechanical state space, where the distance is not necessarily a distance in the metric sense. Consider a set of states represented by Ω density matrices in a $2 \otimes 2$ Hilbert space such that Ω contains a subset of separable states, \mathcal{S} , and a subset of entangled states, $\Sigma = \Omega - \mathcal{S}$. The entanglement measure $\mathcal{E}(\rho_e)$ of a state $\rho_e \in \Sigma$ is defined as [47]:

$$\mathcal{E}(\rho_e) = \min_{\rho_s \in \mathcal{S}} \mathcal{D}(\rho_e, \rho_s) \quad (1)$$

where ρ_e and ρ_s denote the density matrix associated with entangled and separable states respectively.

Out of the several possibilities that could be used to define such a distance \mathcal{D} , Witte et al. [49] used the Hilbert-Schmidt norm as a measure of the distance \mathcal{D} to calculate the entanglement measure $\mathcal{E}(\rho_e)$ as:

$$\mathcal{E}(\rho_e) = \min_{\rho_s \in \mathcal{S}} \|\rho_s - \rho_e\|^2 \quad (2)$$

Witte et al. [49] also showed that $\mathcal{E}(\rho_e)$ is a good measure of entanglement satisfying the various requirements of an entanglement measure.

Using the Hilbert-Schmidt norm, del Cima et al. [50] showed the entanglement measure to be:

$$\mathcal{E}(\rho_e) = 2\epsilon_0 \max(0, |z| - v) \quad (3)$$

where z and ν are the matrix element of reduced density matrix ρ_e and ρ_s and ϵ_0 is a normalization constant to ensure that the entanglement measure $\mathcal{E}(\rho_e)$ satisfies:

$$0 \leq \mathcal{E}(\rho_e) \leq 1$$

. and In order to calculate this measure for a dimer system, we consider the Hamiltonian for a spin 1/2 Heisenberg antiferromagnetic dimer chain that is given by:

$$H = -J \sum_{i=1}^{N/2} (\vec{S}_{i-1} \cdot \vec{S}_i + \alpha \vec{S}_i \cdot \vec{S}_{i+1}) \quad (4)$$

where $J < 0$ represents the exchange coupling constant between a spin at the i^{th} site and its nearest neighbour spin at the $(i-1)^{th}$ site while αJ represents the exchange interaction between the same i^{th} spin but with the other nearest $(i+1)^{th}$ neighbour. \vec{S}_{i-1} , \vec{S}_i and \vec{S}_{i+1} represent the spin operators on the $(i-1)^{th}$, i^{th} and $(i+1)^{th}$ lattice sites respectively. N denotes the number of sites in the dimer. In terms of α , the energy gap is defined as [51]:

$$\Delta = J_1(1 - \alpha)^{\frac{3}{4}}(1 + \alpha)^{\frac{1}{4}} \quad (5)$$

where $0 \leq \alpha \leq 1$.

For a dimer, $\alpha = 0$. Considering a bipartite system where one sub-system is a dimer and the second sub-system is the remaining lattice, equation 4 can be rewritten as:

$$H = -J \vec{S}_1 \cdot \vec{S}_2 \quad (6)$$

In terms of the spin matrices S^x , S^y and S^z , equation 6 becomes:

$$H = -J (S_1^x S_2^x + S_1^y S_2^y + S_1^z S_2^z) \quad (7)$$

Moreover, $S_i^\alpha = \frac{1}{2} \sigma^\alpha$ where σ is the Pauli's matrix. Considering $\hbar = 1$, equation 7 can be written in the matrix form as:

$$H = \begin{pmatrix} -\frac{J}{4} & 0 & 0 & 0 \\ 0 & \frac{J}{4} & -\frac{J}{2} & 0 \\ 0 & -\frac{J}{2} & \frac{J}{4} & 0 \\ 0 & 0 & 0 & -\frac{J}{4} \end{pmatrix}, \quad (8)$$

having the eigenvalues $\lambda_1 = -\frac{J}{4}, \lambda_2 = -\frac{J}{4}, \lambda_3 = \frac{J}{4}, \lambda_4 = \frac{J}{4}$

The corresponding eigenvectors are:

$$|\phi_1\rangle = |00\rangle \quad (9)$$

$$|\phi_2\rangle = |11\rangle \quad (10)$$

$$|\phi_3\rangle = -|01\rangle + |10\rangle \quad (11)$$

$$|\phi_4\rangle = |01\rangle + |10\rangle \quad (12)$$

The reduced density matrix is given by

$$\rho_e = \frac{1}{Z} \sum_i e^{-\beta\lambda_i} |\phi_i\rangle\langle\phi_i|,$$

where Z is the partition function given by

$$Z = 3e^{\frac{J}{4k_B T}} + e^{-\frac{3J}{4k_B T}} \quad (13)$$

$\beta = 1/k_B T$ and k_B is the Boltzmann constant.

In matrix form

$$\rho_e = \frac{1}{Z} \begin{pmatrix} v & 0 & 0 & 0 \\ 0 & w & z & 0 \\ 0 & z^* & w & 0 \\ 0 & 0 & 0 & v \end{pmatrix}, \quad (14)$$

with

$$v = \frac{1}{Z} e^{\frac{\beta J}{4}},$$

$$z = \frac{1}{Z} e^{-\frac{\beta J}{4}} \sinh\left(\frac{\beta J}{2}\right)$$

In terms of the correlations between the spins in an isotropic system [22]

$$v = \frac{1}{4} (1 + 4\langle s_i^z s_{i+1}^z \rangle),$$

$$z = \langle s_i^x s_{i+1}^x \rangle + \langle s_i^y s_{i+1}^y \rangle,$$

From equation 3, it can be seen that the system will present entanglement when

$$v < |z|$$

In terms of the system's partition function:

$$v = \frac{1}{Z} e^{\frac{J}{4k_B T}}, \quad (15)$$

$$z = \frac{1}{Z} e^{-\frac{J}{4k_B T}} \sinh\left(\frac{J}{2k_B T}\right) \quad (16)$$

From equations 3, 15 and 16, we get the distance between the states (\mathcal{D}) entanglement measure, $\mathcal{E}(\rho_e)$, for a dimer system as:

$$\mathcal{E}(\rho_e) = \max\left[0, \left(\frac{1 - 3e^{\frac{J}{k_B T}}}{1 + 3e^{\frac{J}{k_B T}}}\right)\right] \quad (17)$$

From equation 17, it can be seen that the entanglement, $\mathcal{E}(\rho_e)$, is zero for ferromagnetic dimers ($J > 0$). Furthermore, the entanglement temperature, T_E , at which entanglement goes to zero is:

$$T_E = -\frac{J}{k_B \ln 3} \quad (18)$$

1. Equivalence between distance between the states entanglement and Concurrence

Wootters et al. [19] calculated the concurrence of a spin dimer system as:

$$C = \max\{0, \lambda_1 - \lambda_2 - \lambda_3 - \lambda_4\} \quad (19)$$

where λ_i are the square roots of the eigenvalues of $\rho\tilde{\rho}$ in descending order such that $\tilde{\rho}$ is the spin-reversed density matrix, defined by $\tilde{\rho} = (\sigma^y \otimes \sigma^y)\rho^T(\sigma^y \otimes \sigma^y)$, (\dots) and the supercript T indicates transposition.

Thus, the concurrence was found to be

$$C = 2\max(0, |z| - v)$$

which is exactly the same as equation 3.

2. $\mathcal{E}(\rho_e)$ in terms of magnetic susceptibility

To find realistic systems where bipartite entanglement exists at finite temperatures, it would be useful if the distance between the states measure, $\mathcal{E}(\rho_e)$, could be expressed in terms of experimentally accessible quantities like magnetic susceptibility and specific heat.

In order to relate bipartite entanglement in a dimer with magnetic susceptibility, we use the Bleaney-Bowers equation given by [41]:

$$\chi = \frac{2N_A(g\mu_B)^2}{k_B T \left(3 + e^{\frac{-J}{k_B T}}\right)} \quad (20)$$

where N_A is the Avogadro number, g is the Landé's factor and μ_B is the Bohr magneton. The concurrence for such a system was calculated by Aldoshin et al. [?] as:

$$C = \max \left[0, 1 - \frac{3\chi}{\chi_{Curie}} \right] \quad (21)$$

where

$$\chi_{Curie} = \frac{N_A(g\mu_B)^2}{k_B T}$$

From the above section, we found the equality of the distance between the state measure, $\mathcal{E}(\rho_e)$, and concurrence C . Hence, equation 21 becomes:

$$\mathcal{E}(\chi) = \max \left[0, 1 - \frac{3\chi}{\chi_{Curie}} \right] \quad (22)$$

3. $\mathcal{E}(\rho_e)$ in terms of specific heat

The specific heat per mole of a system in a canonical ensemble with partition function Z can be written as:

$$c_m = \frac{\partial(k_B N T^2 \frac{1}{Z} \frac{\partial Z}{\partial T})}{\partial T} \quad (23)$$

For a magnetic spin 1/2 dimer system having a partition function Z given by equation 13, the magnetic specific heat becomes:

$$c_{Mag}(T) = 12k_B N \left(\frac{\beta J}{2}\right)^2 \frac{e^{\beta J}}{(1 + 3e^{\beta J})^2} \quad (24)$$

From equation 17, $e^{\beta J}$ can be expressed in terms of distance between the states as:

$$e^{\beta J} = \frac{1 - \mathcal{E}}{3(1 + \mathcal{E})} \quad (25)$$

Substituting equation 25 in equation 24, the distance between the state measure, $\mathcal{E}(\rho_e)$, can be expressed in terms of specific heat as:

$$\mathcal{E}(C_{Mag}) = \begin{cases} \max \left[0, \sqrt{1 - \frac{4C_m}{k_B N (\beta J)^2}} \right], & \text{for } T < T_E \\ 0, & \text{for } T \geq T_E \end{cases} \quad (26)$$

III. COMPUTATIONAL DETAILS

Interatomic distances and monomeric form of the crystal geometry were calculated with density functional theory (DFT)[69] using Gaussian 16 program package without any constraint on the geometry [69]. The structural parameters (atomic coordinates, inter-atomic distances etc.) obtained from SCXRD measurements were input to the Gaussian 16 program. DFT calculations have been done on the crystal for geometric optimization and simulation of Raman and IR spectrum by Becke three-parameter Lee Yang Parr functional correlation (B3LYP), a well-known functional in DFT for calculating exchange-correlation energy [32, 33]. To correctly incorporate the effect of a metal centre (Cu^{2+}) and organic ligands (oxalate and acetate), we used a dual basis, with LANL2DZ for the metal centre and 6-311++G(d,p) for the rest of the atoms (organic part) [43–46]. Energy minimized monomer unit obtained from DFT calculations was used to compute harmonic infrared vibrational frequencies as well as Raman frequencies and for the structural analysis. The calculations converged to an optimized geometry since there were only real harmonic vibrational wavenumbers, revealing the localization of energy minima. To study the chemical bonding and the magnetic interaction pathway, delocalisation indexes were calculated. Delocalisation index measures the extent of electron’s delocalisation [53] from one atomic space to another atomic space due to interatomic interactions. Optimised geometry from DFT calculation has been used to calculate electron density by Quantum Theory of Atoms In Molecule (QTAIM) using Multiwfn 3.8 software[52].

IV. EXPERIMENTAL SECTION

A. Materials and General Methods

The materials required for the synthesis of copper acetate were purchased commercially and used as-received: 4-Aminopyridine (Merck-Aldrich, 99%), CuCl_2 (Alfa Aesar, 97%), Acetic acid (Merck-Aldrich, reagent grade). The crystals were grown in Memmert’s incubator (Model No. IPP30 PLUS 32L). Thermogravimetric analysis (TGA) and differential scanning calorimetric analysis (DSC) measurements were done in TA Instruments thermal analyzer (Model no. SDT Q600) till 650 °C at a heating rate of 5°C/min under nitrogen environment. Fourier-transform infrared spectroscopy (FTIR) in the range of 400 cm^{-1} -

4000 cm^{-1} with 0.5 cm^{-1} resolution, was done on Shimadzu's spectrometer (Model No. IRPrestige-21) using the KBr pellet technique. Raman spectra were recorded with T64000 spectrophotometer using the 514.5 nm Ar–Kr laser excitation. Magnetisation measurements were done on a 3.4 mg crystal on Quantum Design's physical property measurement system (PPMS)-Model Evercool-II, in the temperature range 1.8 K to 400 K. The measurements were done in the zero field cooled (ZFC) state where the sample was cooled to the lowest temperature in zero field and then a field applied. Magnetisation measurements were performed while warming up the sample. Specific heat measurements were also done using PPMS in the temperature range from 2 K to 270 K. For the measurements, the platform was thermally attached to a temperature bath, and the sample, which has a mass of 3 mg, was thermally connected to it using Apiezon N grease. Specific heat was measured using the thermal relaxation approach, which involves applying a short heat pulse to the sample and extracting specific heat from exponential curve fits to the heating and cooling data.

B. Synthesis

Single crystals of copper acetate were synthesised using the technique of slow evaporation. The technique entails the slow evaporation of solvent from a solution until supersaturation resulting in crystallisation of excess solute [27]. In our technique of slow evaporation, the solvent had two components: (i) a solution A of CuCl_2 dissolved in distilled water and (ii) a solution B of 4-Aminopyridine dissolved in distilled water. It was found that as soon as the two solutions A and B were mixed together, the solutes in each solution precipitated resulting in no crystal formation (see Fig. 1 (c)). To inhibit the precipitation, we decided to add an acidic medium to the solution that would give H^+ ions to the system. Since acetic acid is a weak acid with a pK_a of 4.76, we added acetic acid to the solution. As expected, after addition of acetic acid, the precipitation of the solvents was arrested and a clear blue solution formed (Fig. 1 (d)). This solution was, then, left for slow evaporation.

To initiate slow evaporation, solution A was made by dissolving 0.17g of CuCl_2 in distilled water. Similarly, solution B was made by dissolving 0.37g of 4-Aminopyridine in distilled water. The two solutions were, then, mixed together in a beaker. Small volumes of acetic acid was added slowly to the mixed solution A and B while constantly stirring until the precipitates dissolved completely and a clear blue solution obtained as shown in Fig. 1

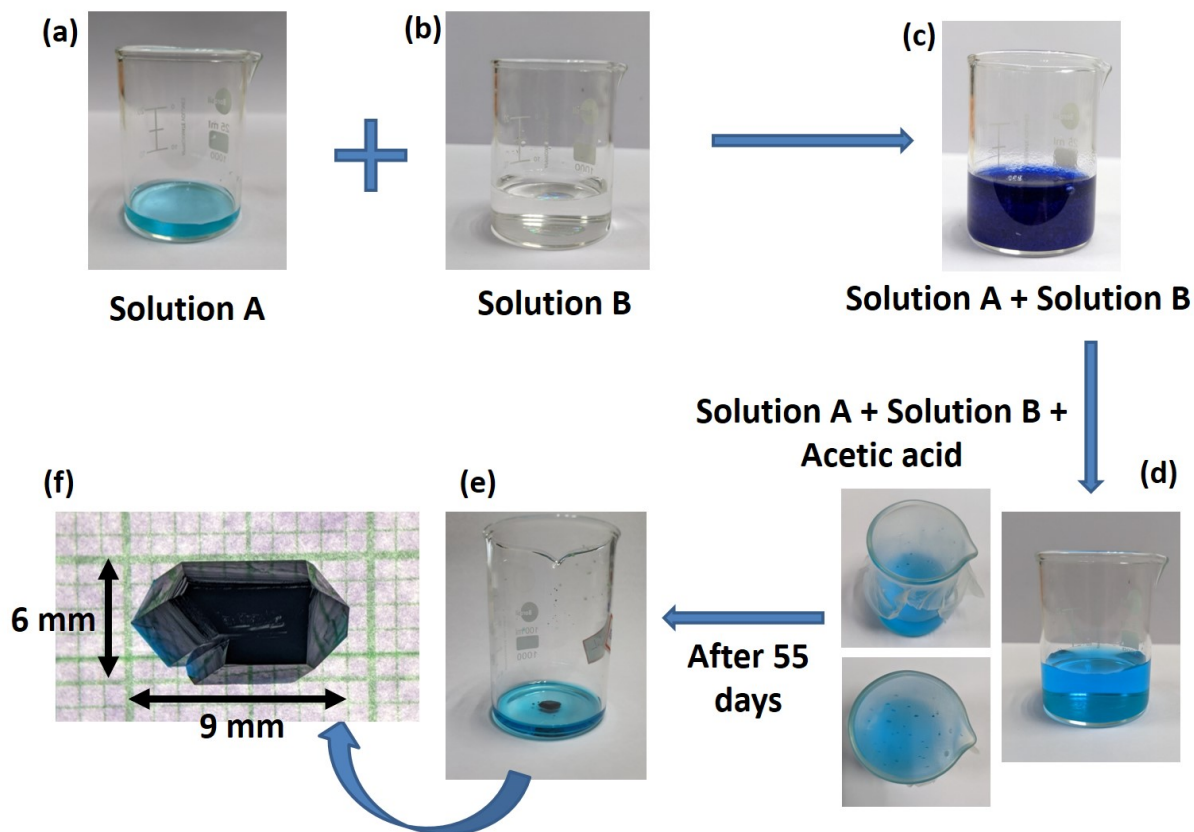


FIG. 1. (colour online) (a) Solution A of CuCl_2 in water (b) Solution B of 4-Aminopyridine in water. (c) Mixture of solutions A and B. (d) Growth solution after adding acetic acid to the mixed solutions A and B. (e) Crystal formation in growth solution. (e) A large sized crystal with hexagonal morphology shown on a graph paper for comparison.

(d). The obtained blue solution was allowed to evaporate slowly at room temperature in an incubator with the top covered with paraffin and few holes punctured on the paraffin. After 40 days, the first tiny crystal nucleated. With the passage of time, this crystal increased in size due to addition of secondary crystallites. After another 15 days, the crystal growth process ended with the formation of a large single crystal (see Fig. 1 (e)) implying that the initial supersaturation attained in the mixture of solutions A and B was low [27]. The crystal growth run gave us 63% yield. The morphology of the large sized crystals was hexagonal (see Fig. 1 (f)). The size of each side of the hexagon was ~ 3 mm with a thickness of ~ 0.3 mm, while the dimension of the rectangular crystals was 10 mm x 10 mm x 0.3 mm. The obtained crystals were washed in minimal amount of cold distilled water and the remaining excess

solvent blotted on a clean tissue paper. The large single crystal was cut to an approximately rectangular shape of dimension 1 cm x 1 cm x 0.3 cm for other measurements. Our objective in taking 4-Aminopyridine as the starting reagent for the crystal synthesis was to use it either as a bridging ligand or a side ligand in order to engineer an exchange interaction between the Cu^{2+} ions. However, structure solution (discussed below) revealed that copper acetate did not contain any aminopyridine.

C. X-ray data collection and structure determination

A tiny prismatic single crystal of dimensions 0.25 x 0.12 x 0.05 mm³ was mounted on the goniometer of Bruker's Kappa APEX II CCD diffractometer equipped with graphite-monochromatized Mo-K α radiation having a wavelength $\lambda = 0.71073 \text{ \AA}$ at room temperature (296(2) K). The intensity data was collected using ω and ϕ scans with frame width of 0.5°. The frame integration and data reduction were performed using Bruker's SAINT/XPREP software [9]. Multi-scan absorption corrections were applied to the data using SADABS (Bruker 1999) [10] program. Intensity distribution indicated a monoclinic structure with the space group as C 2/c, which was confirmed by a successful refinement. Accurate unit cell parameters and orientation matrix were determined by least-squares treatment of the setting angles of 5689 reflections, of which 1233 reflections were independent, in the $2.947^\circ \leq 2\theta \leq 24.996^\circ$ range. The minimum and maximum normalized transmission factors were 0.772 and 0.926. Atomic positions were located by Direct Methods with the structure solution program SHELXT [38] and were then refined by full-matrix least-squares calculations based on F2 using the program SHELXL [39]. Selected crystallographic data is given in the Table I. From the Table I, it can be seen that the goodness of fit R has a low value of 1.117 indicating an extremely good quality of the grown crystal.

V. RESULT AND DISCUSSION

A. Crystal structure

Copper acetate crystallises in the monoclinic system with half the number of molecules in the asymmetric unit. The two halves are related to each other by a centre of inversion. Fig. 2 (a) shows the asymmetric unit obtained from SCXRD measurements. From the figure, it

TABLE I. Selected crystallographic data of $C_8H_{16}Cu_2O_{10}$ obtained from single crystal X-ray diffraction.

Empirical formula	$C_8H_{16}Cu_2O_{10}$
Formula weight	399.31
Crystal System	Monoclinic
Space Group	C 2/c
Unit cell dimensions	a = 13.1585(8) Å b = 8.5575(5) Å c = 13.8517(9) Å $\alpha = 90^\circ$ $\beta = 117.035(2)^\circ$ $\gamma = 90^\circ$
Volume	1389.32(15) Å ³
Z	4
Density (calculated)	1.909 Mg/m ³
Absorption coefficient	3.106 mm ⁻¹
Index ranges	-15<=h<=15, -10<=k<=10, -16<=l<=13
Goodness-of-fit on F ²	1.117
Final R indices [I > 2σ(I)]	R1 = 0.0221, wR2 = 0.0550
R indices (all data)	R1 = 0.0265, wR2 = 0.0571
Extinction coefficient	0.0187(7)
Largest diff. peak and hole	0.421 and -0.227 e.Å ⁻³

can be seen that the asymmetric unit contains 2 Cu atoms, Cu1 and Cu2. Each Cu atom is penta-coordinated with oxygen atoms: Cu1 with O1, O2, O3, O4 and O5; Cu2 with O6, O7 O8, O9 and O10. Four of these O atoms arise from the acetate ligand CH_3COO^- . It is interesting to note that out of the two O atoms in a given acetate ligand, one (for instance, O4) is co-ordinated with Cu1 atom while the other O atom (O9) is co-ordinated with Cu2 atom. The fifth penta-coordinated O atom with Cu atom arises from a water molecule:

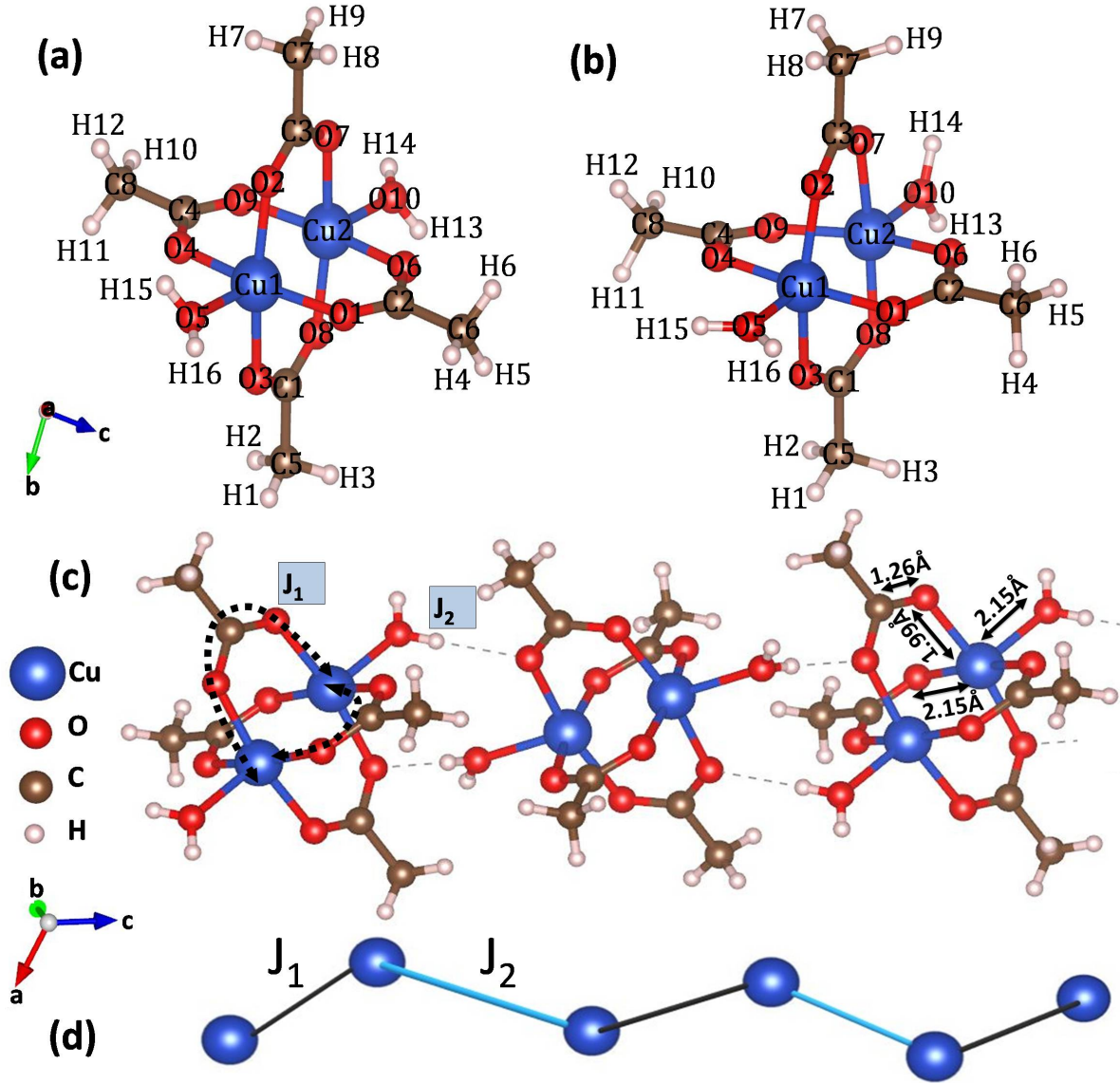


FIG. 2. (colour online) (a) Asymmetric unit of $C_8H_{16}Cu_2O_{10}$ obtained from single crystal X-ray diffraction. (b) Optimized geometry of $C_8H_{16}Cu_2O_{10}$ generated by the dual basis (see text for details). (c) Atomic labeling is shown.

H15-O5-H16 with Cu1 and H13-O10-H14 with Cu2 atom. Four acetate ligands CH_3COO^- , each with a net negative charge warrants that the oxidation state of Cu in copper acetate is Cu^{2+} , ensuring that the total charge on an asymmetric unit is zero making the molecule neutral. Lattice parameters obtained from SCXRD data are given in the Table II.

Monomeric unit pertaining to the optimised geometry of copper acetate obtained from the

Experiment Theory			Experiment Theory		
Bond length[Å]		Bond angle[°]			
Cu1-Cu2	2.61(7)	2.73	O2-Cu1-O4	89.21(7)	89.14
Cu1-O1	1.95(19)	2.04	O3-Cu1-O5	93.05(8)	93.41
Cu1-O2	1.98(15)	1.99	O3-Cu1-O1	89.21(7)	89.14
Cu1-O3	1.99(15)	1.99	O1-Cu1-O2	90.98(7)	89.72
Cu1-O4	1.93(3)	2.04	O4-Cu1-O5	97.68(9)	99.52
Cu1-O5	2.15(3)	2.14	O2-Cu1-O5	98.29(8)	93.41
Cu2-O6	1.93(3)	1.99	O2-Cu1-O3	168.63(10)	173.17
Cu2-O7	1.99(15)	2.04	O1-Cu1-O4	168.66(10)	160.95
Cu2-O8	1.98(15)	2.04	Cu1-O5-H15	134.00(3)	123.10
Cu2-O9	1.95(19)	1.99	O7-Cu2-O8	168.63(10)	160.93
Cu2-O10	2.15(3)	2.14	O9-Cu2-O6	168.66(10)	173.16
			O7-Cu2-O10	93.05(8)	99.53
			O8-Cu2-O10	98.29(8)	99.53
			O7-Cu2-O6	90.25(8)	89.71
			O7-Cu2-O9	90.98 (8)	89.15
			O8-Cu2-O6	97.34(8)	89.15
			O9-Cu2-O8	90.98(7)	89.71
			Cu2-O10-H13	134.00(3)	123.10
			Cu2-O10-H14	114.00(3)	123.10

TABLE II. Comparison of experimentally obtained SCXRD crystallographic data of $C_8H_{16}Cu_2O_{10}$ with that obtained from DFT calculations.

DFT calculations employing the dual basis set as described in the above section is shown in Fig. 2 (b). From Figs. 2 (a) and (b), it is apparent that the experimentally obtained asymmetric unit and the monomeric unit obtained from DFT calculations are equivalent. Bond lengths corresponding to the magnetic copper atom are given in the Table II. From the table, it can be seen that an excellent match of the experimentally obtained bond lengths exists with those of the theoretically obtained one resulting in negligible discrepancies with the experimental geometry in the bond lengths. It is to be remembered that the calculations

were performed without any constraint on the geometry unlike [53] where calculations were done on a fixed geometry to minimise the differences in the computationally and experimentally obtained bond lengths. This suggests that our dual basis incorporating both the metal and organic parts is a good basis to describe the structure of copper acetate. Bond angles of copper with oxygen of the kind O-Cu-O is also very good and those with oxygen and hydrogen atoms of the kind Cu-O-H is reasonably good. Considering the fact that the DFT calculations are done on a single molecule of copper acetate that is assumed to be in a gaseous state, the good match with experimentally and theoretically obtained data implies that the actual crystalline state of copper acetate may comprise one dimensional chains of copper that are magnetically isolated in the other two directions due to weak interchain interactions.

The molecular chain structure of copper acetate obtained from the SCXRD data is shown in Fig. 2 (c). The crystal is composed of a chain of units of copper linked by H-bonds along the c-axis. Each unit in copper acetate is bound to the neighbouring unit through two hydrogen bonds O-H \cdots O, involving acetate oxygen atoms and water molecules. A unit of copper comprises two copper atoms that are bonded through four acetate groups to form a dimer. The bonds formed by the four acetate groups give the well-known paddlewheel structure to the molecule [68]. Each of the central copper atom is connected to four oxygen atoms from the acetate group and one oxygen atom from the water molecule. The H-bond is shared with the water molecule and adjacent acetate group in the next molecule (see Fig. 2 (c)). Cu ions in the molecule are separated by 2.61 Å, and the intermolecular distance along the c-axis is 5.2 Å. Dimer atoms are connected by H-bond along the b-axis with a separation of 7.2 Å which is larger than the separation in the c-axis. Since the Cu-Cu distance in copper acetate (2.619 Å) is very close to the Cu-Cu distance in metallic copper (2.56 Å), a direct exchange between the two copper atoms seems a big possibility. However, the Cu-O(CO) is distance (2.616 Å) is smaller than the sum of the ionic radii of copper and oxygen atoms implying a covalent bond in copper acetate and a possible superexchange between the copper atoms consequently [54]. In order to confirm if the primary source of magnetic exchange between the copper atoms is via direct exchange or is mediated via oxygen atoms through superexchange, we calculated the delocalisation index, $\delta(A, B) = 4 \int_{\Omega(A)} dr_1 \int_{\Omega(B)} dr_2 \rho(r_1, r_2) - 2N(A)N(B)$, where $\rho(r_1, r_2)$ is the two-particle density for electrons of parallel spin [55]. $\delta(A, B)$ denotes the extent of delocalisation of electrons in an atom A towards the electrons of another atom

B [58] such that a value of unity is attained for bond formation.

Bond pairs	B3LYP
6-311++G(d,p)-LANL2DZ	
Cu-Cu	0.527
Cu-Oac	0.809
Cu-Ow	0.630
O-Hw	0.865
C-C	1.043
C-Oac	1.600
C-H	0.882

TABLE III. Delocalization index for copper acetate calculated using DFT B3LYP with dual basis set 6-311++G(d,p)-LANL2DZ.

Table III depicts the details of the calculated $\delta(A, B)$ for interatomic interactions present in the copper acetate in the basis set, B3LYP/6-311++G(d,p)-LANL2DZ. The estimated DI for C-Oac ($\delta(C, O) = 1.601$) is comparable to the typical DI for π and σ bonds in the acetate molecule (O-C=O), which is 1.5. Similar to what is expected for a covalent bond, the DI values of the O-H, C-C, and C-H bonds are close to 1 [56]. For the C-O bond in the acetate group, there is also a covalent bond with $\delta(C, O) = 0.809$, which is again close to 1. With $\delta(Cu, O) = 0.809$, the covalent bond between copper and oxygen is also close to 1. Given that the interactions in copper acetate are of metal-ligand kind, DI values are lower than that of strong covalent bonds in C-C or C-O. The important point is that the $\delta(Cu, Cu)$ for direct bond yields even smaller values equal to 0.527, which is comparable with the values of similar molecules when no bond pathway is observed [57]. This low value of the $\delta(Cu, Cu)$ bond in comparison to the other $\delta(Cu, O)$, $\delta(C, C)$, $\delta(C, O)$ and $\delta(C, H)$ bonds shows that direct electron sharing between two Cu atoms is unlikely. This also eliminates the possibility of direct magnetic interaction between Cu atoms, providing only the super exchange mediated by Cu-O bonds as the only path to dimer formation.

Since the value of Cu1-O3 and Cu2-O7 is the same at 1.99 Å and Cu1-O5 and Cu2-O10 is same at 2.15 Å (refer Table II), there are two possible exchange pathways for the intradimer connection, namely, Cu1-O3-H14 (at an angle of 116.9°) and Cu2-O7-H15 (at an angle

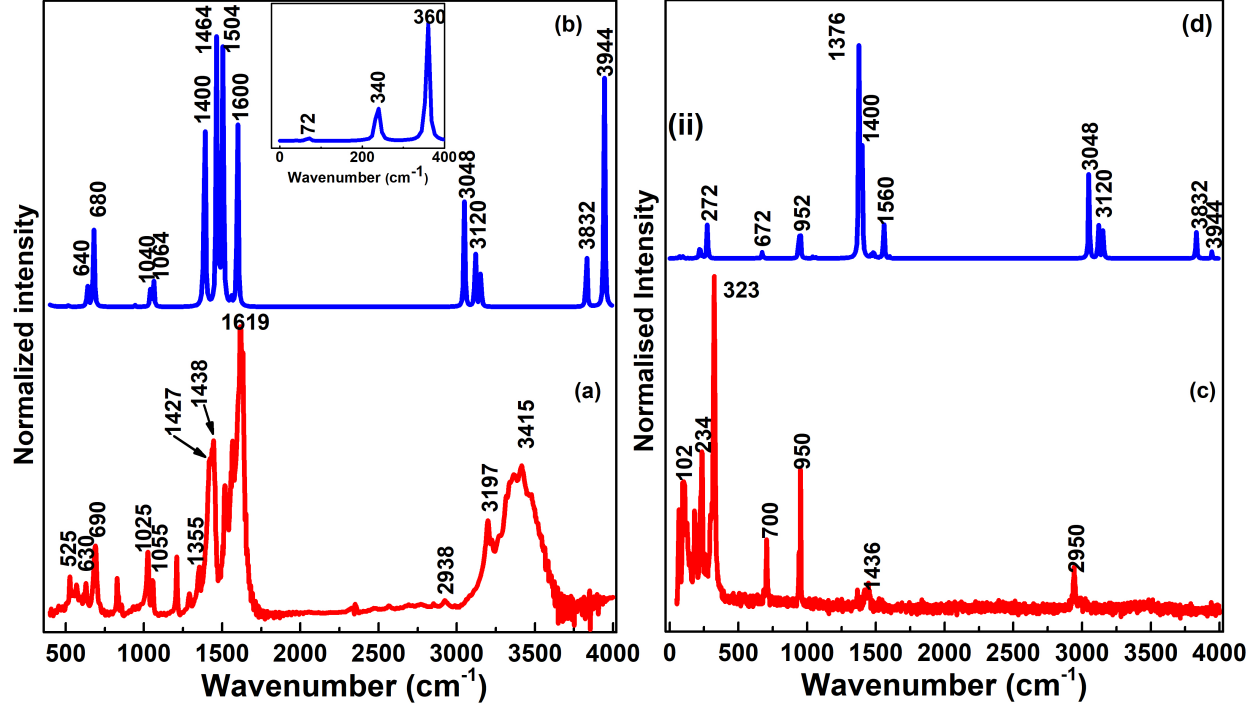


FIG. 3. (a) Red curve is the experimentally obtained room temperature (298 K) FTIR spectrum of $C_8H_{16}Cu_2O_{10}$. (b) Blue curve is the theoretically simulated spectrum using the dual basis. (c) Raman spectrum of $C_8H_{16}Cu_2O_{10}$ obtained experimentally at room temperature (red curve) and (d) Theoretically simulated (blue curve). Frequencies corresponding to relevant vibrations are marked.

of 116.9°). It is clear from the polyhedral chain structure that the dimers (Cu_2-Cu_1 and Cu_2-Cu_1) are not in the same plane along the c -axis and are making a dihedral angle of $94.42(4)^\circ$. These nonplanar bonds give a zig-zag chain structure to the crystal along the c -axis. Due to the two different interactions in intra-dimer and inter-dimer copper ions, a dimeric copper chain is formed, as shown in Fig. 2 (d) having very different values of the exchange coupling constants J and αJ such that αJ is much smaller than J .

1. FTIR and Raman spectroscopy

In order to understand how the theoretically obtained infra red and Raman frequencies compare with the experimentally obtained one, we measured FTIR and Raman spectra of copper acetate and plotted them in Fig. 3. Red curves in Fig. 3 depict the experimentally

obtained spectra while the blue correspond to the theoretically simulated spectra computed on a monomeric unit using the mixed basis (see section above). From the monomeric unit shown above (see Fig. 2 (a-(c))), acetate, water and Cu-O bonds are expected to contribute primarily to the FTIR and Raman frequencies. So, the peaks corresponding to the acetate ligand are observed at frequencies of $\nu_1 = 2938 \text{ cm}^{-1}$ (sym. CH_3 stretch); $\nu_2 = 1427 \text{ cm}^{-1}$ (sym. C-O stretch); $\nu_3 = 1355 \text{ cm}^{-1}$ (sym. CH_3 bend); $\nu_4 = 1619 \text{ cm}^{-1}$ (asym. C-O stretch); $\nu_5 = 1438 \text{ cm}^{-1}$ (asym. CH_3 bend); $\nu_6 = 1055 \text{ cm}^{-1}$ (CH_3 asym. bend); $\nu_7 = 1025 \text{ cm}^{-1}$ (CH_3 rocking); $\nu_8 = 690 \text{ cm}^{-1}$ (sym. COO bending) and $\nu_9 = 630 \text{ cm}^{-1}$ (COO rocking) in the FTIR spectrum of Fig. 3 (a).

The FTIR spectrum of copper acetate also exhibits strong absorption in the regions of the stretching vibrations of coordinated water molecules as evident in the intense peaks at 3415 cm^{-1} [54], 3197 cm^{-1} and 1619 cm^{-1} (scissoring (H_2O)) [?] of Fig. 3 (a). The expected magnetic interaction between the two copper atoms mediated by the paddlewheel arrangement of Cu-O atoms (dotted curve in Fig. 2 (c)) should result in a peak in the FTIR spectrum at a Cu-O frequency. Indeed, the low intensity peaks at 525 cm^{-1} , 590 cm^{-1} and 628 cm^{-1} are observed in Fig. 3 (a) confirming the presence of Cu-O vibrations in copper acetate [60, 61].

The theoretically simulated FTIR spectrum using the mixed basis shows a very good match of the calculated frequencies with the experimentally obtained ones as shown in Fig. 3 (b), proving the usefulness of the mixed basis for DFT calculations of metal-organic compounds. It is to be noted that some of the IR frequencies corresponding to Cu-O vibrations are present below 500 cm^{-1} [62]. Due to experimental constraints of our instrument that has a poor resolution of the frequencies below 500 cm^{-1} , we were unable to measure these frequencies. However, an indication of the contribution of these frequencies to the IR spectrum of copper acetate was obtained from the DFT simulated IR spectrum as shown in the inset of Fig. 3 (b) where frequencies at $\nu_s = 72 \text{ cm}^{-1}$ (Cu-Cu-O bending), $\nu_s = 340 \text{ cm}^{-1}$ (O-C-uO bending) and $\nu_s = 360 \text{ cm}^{-1}$ (sym. CuO stretch) are observed [62].

In order to confirm the low frequency bands associated with Cu-O, we performed Raman spectroscopy on copper acetate in the range of 50 cm^{-1} to 4000 cm^{-1} as shown in Fig. 3 (c). Vibrations of the acetate ligand are observed at $\nu_1 = 1436 \text{ cm}^{-1}$ (asym. CH_3 bending); $\nu_2 = 950 \text{ cm}^{-1}$ (sym. CCH_3 stretching) and $\nu_3 = 700 \text{ cm}^{-1}$ (sym. COO bending) [62]. Unlike the FTIR spectrum, the Raman spectrum presents clear peaks in the low frequency range

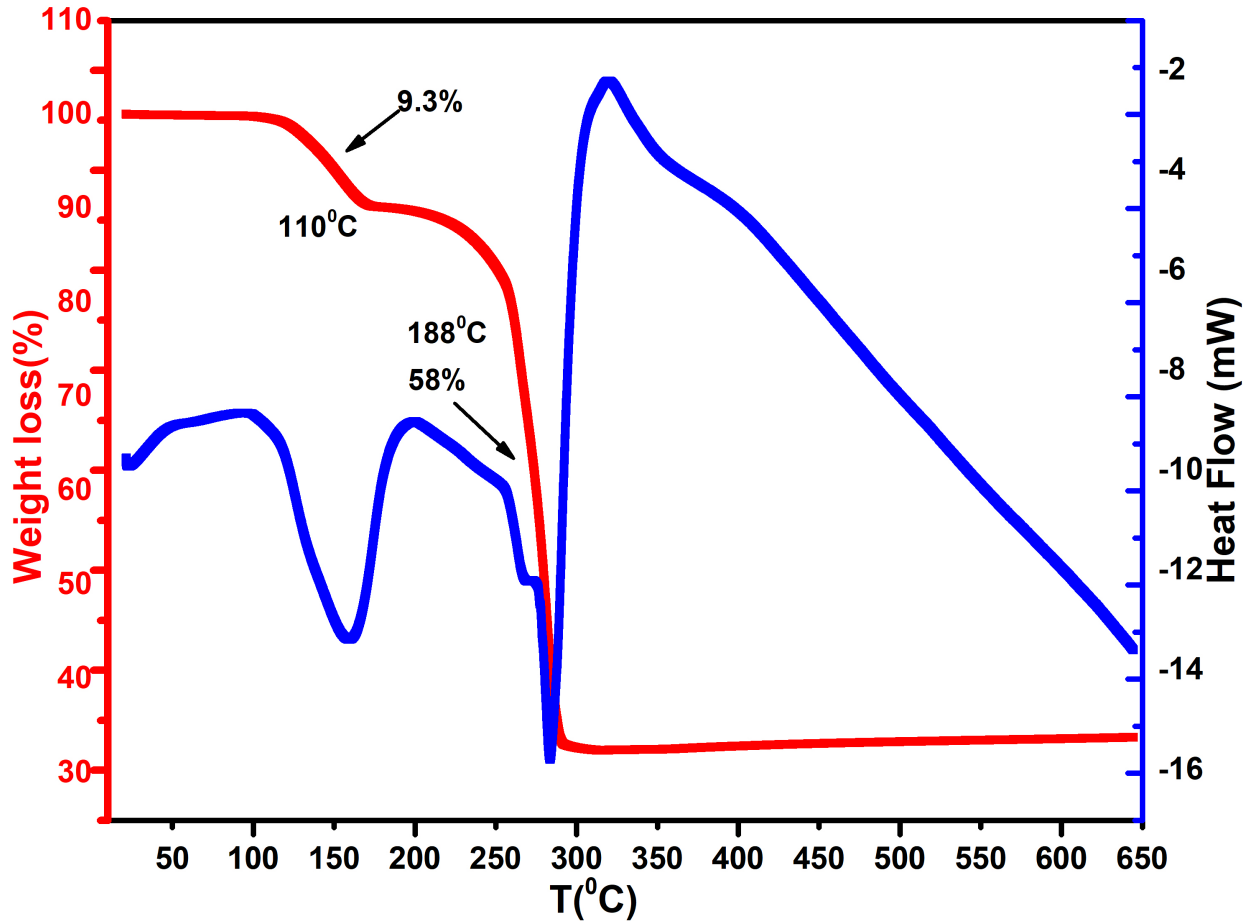


FIG. 4. TGA (red) and DSC (blue) curves of copper acetate showing two distinct weight losses.

where frequencies corresponding to Cu-O vibrations are seen at $\nu_4 = 323 \text{ cm}^{-1}$ (sym. CuO stretching); $\nu_5 = 234 \text{ cm}^{-1}$ (O-Cu-O bending) and $\nu_6 = 102 \text{ cm}^{-1}$ (Cu-Cu-O_w bending). Fig. 3 (d) shows the simulated Raman spectrum obtained using the mixed basis. As can be observed from the spectrum, a good match is obtained between the experimentally obtained and theoretically simulated spectra.

2. Thermal Analysis

The copper acetate crystal was subjected to TGA and DSC measurements to ascertain its thermal stability. The TGA data collected in the 20°C to 640°C temperature range is represented as a red curve in Fig. 4. Blue curve in Fig. 4 shows the DSC measurement that was carried out simultaneously to determine the nature of the underlying change (en-

dothermic or exothermic). It was found that the weight reduction happens in two stages. First, a weight loss of 9.3% at 110°C is observed accompanied by a small endothermic peak. The amount of water molecules in the crystal, as a proportion of its weight, is discovered to be about 9.02%. So, it is obvious that the weight loss is a result of dehydration. The slight difference between the measured mass loss and the absolute dehydration value predicted by theory for $C_8H_{16}Cu_2O_{10}$ suggests that other mechanisms causing mass loss take place in this temperature range. One of such possible events is the oxidation of the sample's surface to form copper acetate peroxides [63]. Impure nitrogen containing a small quantity of oxygen can make copper acetate peroxides since they just need a small amount of oxygen to form. Due to their instability, these peroxides start to break down at low temperatures (below 168°C), which causes further mass loss between 110 to 180° besides the dehydration. Second, at 188°C, there is a significant weight loss of about 58%, accompanied by a sizable endothermic peak in the DSC data. This weight loss could be caused by the disintegration of acetate links connecting the copper atoms in the dimer, which has a weight percentage of $\sim 59\%$ [64] when the four clusters forming the paddle wheel structure are considered. The sharp endothermic peak shows that except for the liberation of crystalline water at 110°C, this crystal is stable up to 188°C without any phase transition [43].

B. Bipartite entanglement

1. *via magnetic susceptibility*

From the delocalisation index calculations above as well as the IR and Raman measurements above, it is clear that the exchange interaction happens through the paddlewheel structure formed via the acetate group rather than the direct Cu-Cu exchange. In order to ascertain the formation of a dimer ground state and a consequent estimation of bipartite entanglement via the distance between the state measure, it is essential to measure magnetic susceptibility as well as specific heat of copper acetate. Black filled circles in Fig. 5 (a) denote the temperature variation of experimentally obtained magnetic susceptibility. From the graph, it is clear that a broad peak exists at a temperature $T_p \sim 260$ K, similar to other published works [28, 66] and indicative of low dimensionality. The figure also presents a low temperature upturn that starts below ~ 50 K and rises sharply below 20

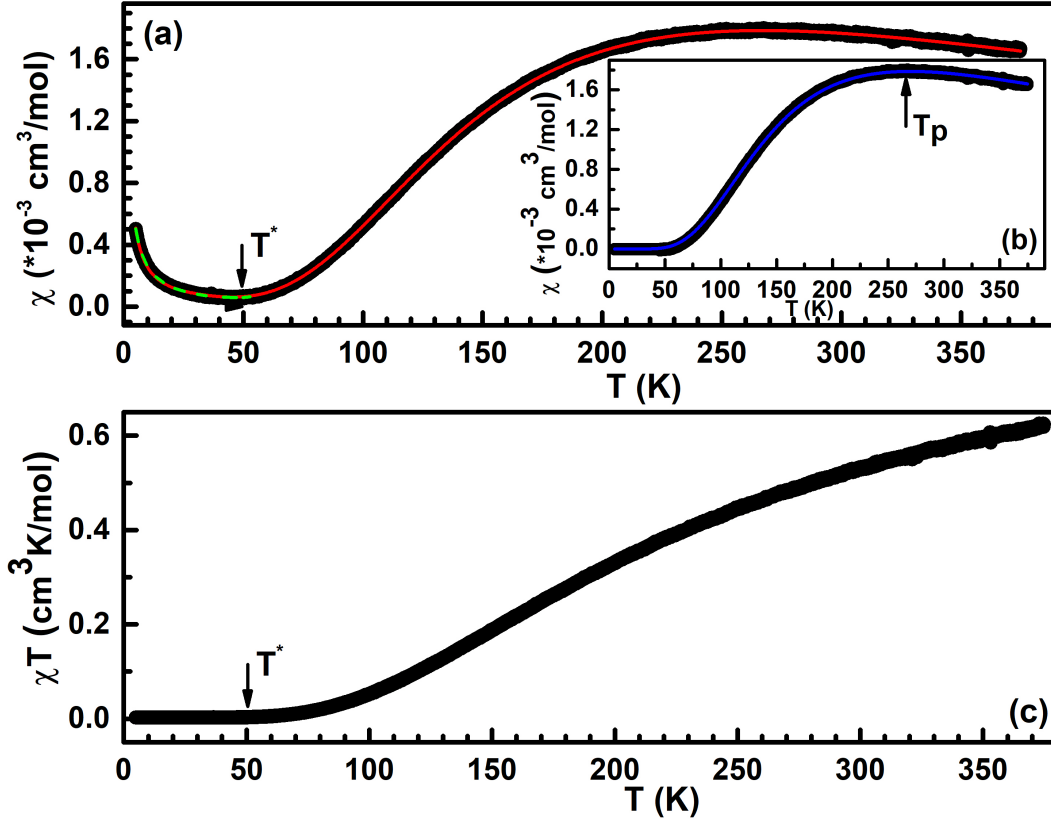


FIG. 5. (a) Black filled circles represent the temperature variation of magnetic susceptibility at an applied field of 50 mT. Red curve is a fit to a 1D Heisenberg alternating chain model. Green dashed line is a fit to the equation $\chi(T) = \chi_0 + \chi_{CW}(T) + \chi_{spin}(T)$. (b) Black filled circles represent the temperature variation of magnetic susceptibility after subtracting the uncoupled spin contribution to the data. Blue curve is a fit to the Bleaney Bowers expression (see text for details). The peak temperature T_p is marked. (c) Temperature variation of χT .

K. Since the expected ground state is that of a dimer, such an upturn may arise due to uncoupled spins arising due to paramagnetic impurities [11]. To confirm this, a fit to a one dimensional Heisenberg alternating chain model was done incorporating impurities due to uncoupled spins (para), alternation parameter (α), Curie constant (CC) and exchange coupling constant (J/k_B) as fit parameters[7]. Red curve in Fig. 5 (a) is the resultant fit with the obtained fit values as para = 0.27%, $\alpha = 0.0017$, CC = 0.95 and $J/k_B = 430$ K. The vanishingly low value of α obtained as a result of an excellent fit to the data implies that the ground state of copper acetate is a dimer as expected. The percentage impurity spins

in our crystal is quite low at 0.27%, however, it is necessary to subtract this paramagnetic contribution in order to obtain the susceptibility of the dimer. To do this, we fitted the data below 50 K (green dashed line in Fig. 5 (a)) to $\chi(T) = \chi_0 + \chi_{CW}(T) + \chi_{spin}(T)$ [11, 51] where χ_0 is a temperature independent term, $\chi_{CW}(T) = C/(T-\theta)$ is the Curie-Weiss term arising due to magnetic impurity and $\chi_{spin}(T) = aT^{-1/2}\exp(-\Delta/k_B T)$ is the spin susceptibility of a one dimensional chain with a finite gap Δ . The obtained fit parameters are as follows: $\chi_0 = -9.4 \times 10^{-5} \text{ cm}^3/\text{mol}$, $C = 0.023 \text{ cm}^3\text{K}/\text{mol}$, $\theta = -0.58 \text{ K}$ and $\Delta/k_B = 352 \text{ K}$. The obtained χ_0 value is close to the value obtained from closed shell diamagnetic susceptibility value $-17.5 \times 10^{-5} \text{ cm}^3/\text{mol}$.

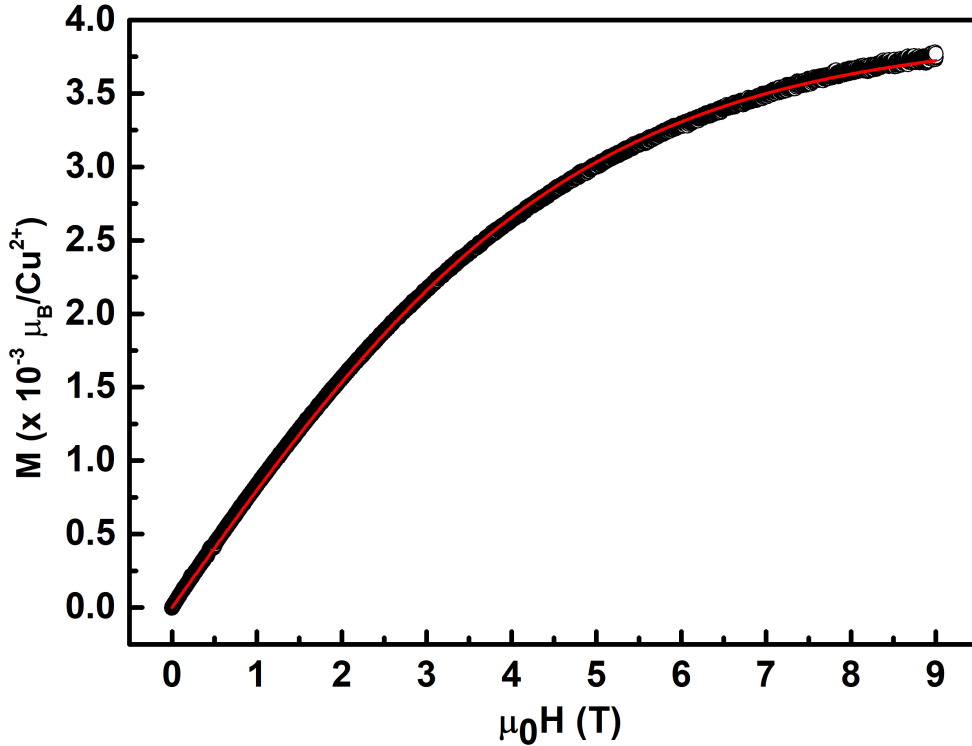


FIG. 6. Black open circles represent the field variation of magnetisation while the red solid curve is a fit to the Brillouin function.

Black curve in Fig. 5 (b) is the magnetic susceptibility of copper acetate obtained after subtracting the impurity contribution arising due to paramagnetic impurities. As can be seen from the figure, the susceptibility vanishes to zero at low temperatures as expected for a dimer ground state due to formation of singlets. To confirm the dimer

ground state, we fitted the susceptibility to Bleaney Bowers expression of the form $\chi(T) = 2Ng^2\mu_B^2/k_B T[3+\exp(\Delta/k_B T)]$ where symbols have their usual meaning. Blue dashed curve in Fig. 5 (b) is the fitted curve which is seen to overlap the experimentally obtained data, confirming the dimer ground state. The obtained fit parameters are $g = 2.17$ and $\Delta/k_B = 426$ K. A final confirmation of the presence of magnetic impurities in the system was obtained by doing a field dependent magnetisation measurement as shown in Fig. 6. Here, the Brillouin function[7]:

$$M_{mol}(B, T) = M_{sat}B_s(g\mu_B SB) \quad (27)$$

$$B_s(g\mu_B SB) = \frac{2S+1}{2S} \coth\left(\frac{2S+1}{2S} \frac{g\mu_B SB}{k_B T}\right) - \frac{1}{2S} \coth\left(\frac{1}{2S} \frac{g\mu_B SB}{k_B T}\right) \quad (28)$$

shown in the red curve is found to fit the data perfectly well in the measured field range of 0 to 9 T. The obtained fit parameter values are $M_{sat} = 3.7$ and $g = 2.9$ where M_{sat} is the saturated magnetisation, S is spin and B is the applied magnetic field.

From equation 21, the distance between the states, \mathcal{E} , is obtained in terms of the product of susceptibility and temperature, so it is informative to plot the temperature variation of $\chi(T)T$ as has been shown in Fig. 5 (c). The susceptibility values correspond to the ones from Fig. 5 (a) without any paramagnetic subtraction. As can be seen from Fig. 5 (c), $\chi(T)T$ decreases monotonically with temperature indicating antiferromagnetic correlations. Below ~ 50 K, $\chi(T)T$ is seen to become a constant, implying paramagnetic behaviour, consistent with the discussions above.

We now, plot the temperature variation of the distance between the states in terms of magnetic susceptibility, $\mathcal{E}(\chi)$, as shown by the filled black circles in Fig. 7. From the figure, it can be seen that $\mathcal{E}(\chi)$ starts from the maximum possible value of 1 [20] at the lowest measured temperature of 1.8 K and starts to decrease steadily with a further increase in temperature. The dimer given by Hamiltonian 6 has two energy levels $+3J/2$ and $-J/2$ separated by the energy gap Δ , where the first level is a singlet and the second is a triply degenerate level. At absolute zero of temperature, the singlet state of copper acetate is completely populated making its spin entanglement correspond to that of a pure and maximally entangled state. As the temperature increases, the triplet state starts to get populated reducing the total entanglement of copper acetate. Very surprisingly, it retains a large finite value of 0.5 at a high temperature of 150 K. With a further increase in temperature, the entanglement value decreases further and reaches an extremely low

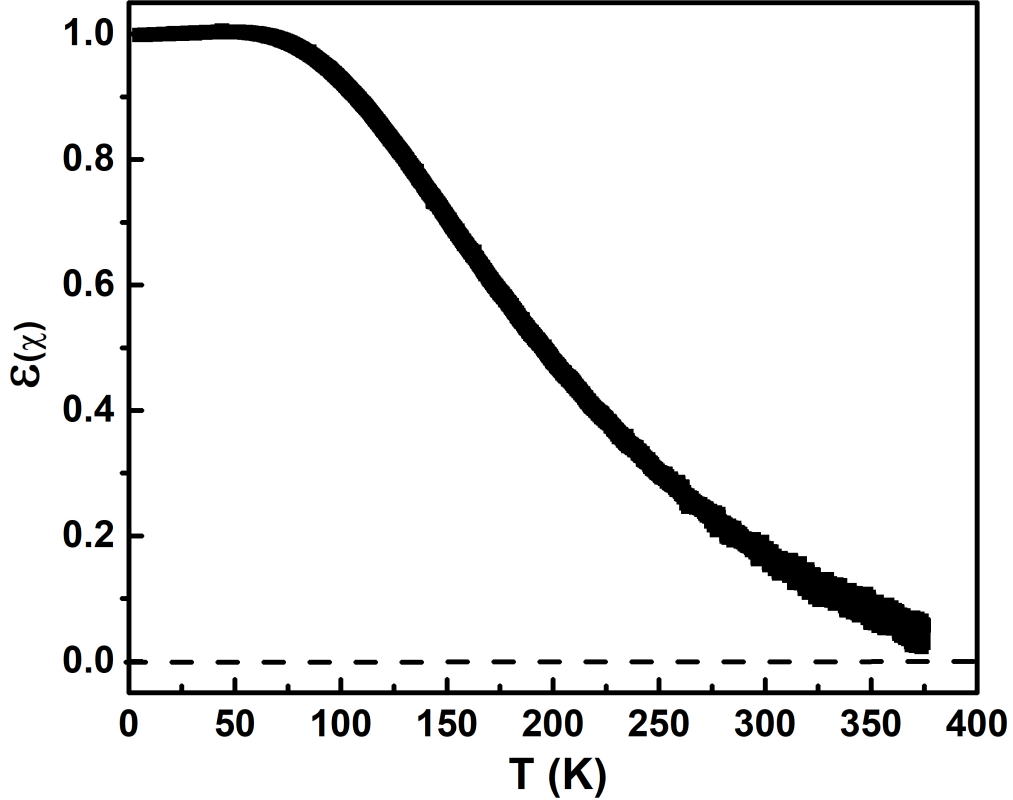


FIG. 7. Temperature variation of distance between the states in terms of magnetic susceptibility, $\mathcal{E}(\chi)$.

value of ~ 0.05 at 380 K. However, it is to be noted that the entanglement has still not reached a zero value. The calculated value of the entanglement temperature, T_E , using the equation 18 is 390 K implying that at this temperature half of the total dimer spins should have been in the triplet state reducing the total entanglement of copper acetate to zero. The presence of finite entanglement even at temperatures equal to the energy gap of the dimer implies that there is some other energy scale in the system that protects the entanglement of the system against decoherence with the surroundings. The fact that this temperature is much above room temperature is quite surprising! To our knowledge, such a high temperature for entanglement existence in a many-body system has not been previously reported. From the magnetic susceptibility measurements, the exchange coupling constant, J/k_B , for the spin dimer has been found to be 430 K. In a recent work, we have shown that

multipartite entanglement in a spin 1/2 uniform-chain system [40] exists at temperatures as high as $2.5J/k_B$. So, it is quite probable that a finite bipartite entanglement exists till at least 430 K in this system as well. Unfortunately, the copper acetate crystal degrades at temperatures larger than 380 K (refer to the TGA discussions above), so we cannot investigate the spin entanglement of this excellent dimer system at temperatures larger than 380 K.

2. via specific heat

In order to compare the distance between the state measure obtained from susceptibility to that obtained from specific heat, we performed specific heat measurements from 3 K to 270 K on copper acetate in zero applied magnetic field as illustrated by the filled black circles in Fig. 8. There are two noteworthy observations from the figure. The first is the observation of a small peak at a temperature of ~ 20 K. Since this temperature is exactly the same as the temperature where the magnetic susceptibility showed an upturn arising due to uncoupled spins (see above), the peak is ascribed to a Schottky anomaly [71].

To confirm that the peak is indeed due to a Schottky anomaly, we fitted the peak using the Schottky equation 29, considering a two-level system with $S = 1/2$, as shown below:

$$C_{Sch} = R \left(\frac{\Delta}{k_B T} \right)^2 \frac{e^{\frac{\Delta}{k_B T}}}{(1 + e^{\frac{\Delta}{k_B T}})^2} \quad (29)$$

where $R = 8.314 \text{ Jmol}^{-1}\text{K}^{-1}$ is the molar gas constant and Δ is the energy separation of the two-level system. The fit using the above equation in the temperature range 3-40 K is shown as a red solid line in Fig. 8 and shown on an expanded scale as the inset (a) of Fig. 8. It can be seen that the red solid line fits the peak at 20 K quite well confirming that the peak arises due to Schottky anomaly arising due to impurities.

To discount the effect of the Schottky anomaly arising due to impurities, we subtracted the specific heat contribution, C_{Sch} , calculated as above and the resultant curve is plotted as black open circles in Fig. 8. We assume that the total specific heat of copper acetate arises due to two different contributions, one due to lattice phonons and the other due to magnetic contribution, C_{Mag} , arising from the thermal population of excited dimer states. To incorporate the effect of lattice phonons, we fitted the temperature variation of $C_{subtracted}$ considering a combined Debye and Einstein model having relative weights of m and $1 - m$

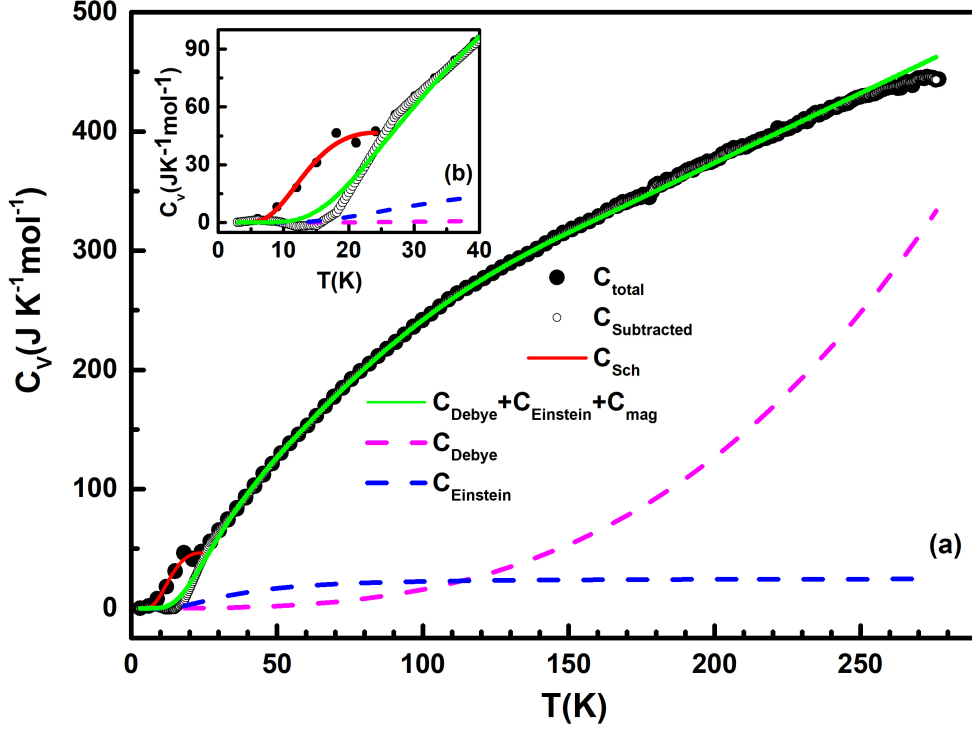


FIG. 8. (a) Black filled circles represent the experimentally obtained specific heat data in zero applied magnetic field. Red solid curve is a fit to the Schottky equation 29 while the open black circles represent the data after the subtraction of the Schottky contribution (see text for details). Green solid line represent the fit to equation 30 while pink and blue dotted lines represent simulated data for contributions due to Debye and Einstein respectively. (b) Expanded data in the temperature range 0 to 40 K to show the Schottky peak clearly.

respectively. The total phonon and magnetic contribution was, then, fitted with relative weights of v and $1 - v$ respectively:

$$C_{subtracted}(T) = v[mC_{Debye}(T) + (1 - m)C_{Einstein}(T)] + (1 - v)C_{Mag}(T) \quad (30)$$

where the first and the second term represent the acoustic and optical phonon mode contribution described by Debye and Einstein models respectively [74]:

$$C_{Debye}(T) = 9R \left(\frac{T}{\theta_D} \right)^3 \int_0^{x_D} dx \frac{x^4 e^x}{(e^x - 1)^2} \quad (31)$$

$$C_{Einstein}(T) = \sum 3R \left(\frac{\theta_{Ei}}{T} \right)^2 \frac{e^{-\frac{\theta_{Ei}}{T}}}{(e^{-\frac{\theta_{Ei}}{T}} - 1)^2} \quad (32)$$

where θ_D and θ_{Ei} represent the Debye and Einstein temperatures respectively. Since a single Einstein term could not fit the entire data, two Einstein terms E_1 and E_2 were needed to fit the data. The third term in equation 30 is the magnetic contribution to the specific heat and is given by equation 24 above. Green solid line in Fig. 8 is the fit to the subtracted data using equation 30. The best fit was obtained for $\theta_D = 487$ K, $\theta_{E1} = 111$ K, $\theta_{E2} = 1275$ K, $v = 0.73$ and $m = 0.39$. The pink and blue dashed lines in the Fig. 8 show the simulated data corresponding to Debye and Einstein contribution respectively. To validate the findings of the fit, these temperatures are compared with optical phonon frequencies obtained by Raman spectroscopy on our dimer (refer to Fig. 3 above). The experimentally obtained highest intensity Raman peak at a frequency of 323 cm^{-1} (see Fig. 3 (c)) has an excellent match with the obtained Debye temperature of 495 K which corresponds to a frequency of 345 cm^{-1} . Similarly, the Raman peak at 950 cm^{-1} matches fairly well with the obtained Einstein temperature $\theta_{E2} = 1275$ K (corresponding to 888 cm^{-1}). The frequency corresponding to the lower Einstein temperature of $\theta_{E1} = 111$ K (corresponding to $\sim 77 \text{ cm}^{-1}$) falls below the measurable limit of the used Raman spectrometer.

To estimate the temperature variation of distance between the states in terms of specific heat, $\mathcal{E}(C_{Mag})$, as given by equation 26, it is necessary to first plot the temperature variation of magnetic contribution to the specific heat obtained from the magnetic fit to the specific heat, C_{Mag} , obtained above. This is plotted as red filled circles in Fig. 9 (a). Evidently, the magnetic contribution to the specific heat is quite small compared to the lattice contribution. Since we did not have a non-magnetic reference material using which the lattice contribution could be estimated, we could not unambiguously extract the magnetic contribution from the measured specific heat. However, since the temperature variation of C_{Mag} is quite similar to that observed in other published dimer systems [12, 72], it is hoped that the temperature variation is of the correct kind. It can be seen that the specific heat value is zero till a temperature of ~ 50 K indicating no density of states at the Fermi level till ~ 50 K since the dimers are in the ground state and the density of triplons is zero. With an increase in temperature, the specific heat increases due to excitation of triplons across the energy gap arising due to the thermal energy. Similar to the observation of a broad peak in magnetic susceptibility at 260 K (see Fig. 5 (a)), we observe a broad maxima in the specific heat at

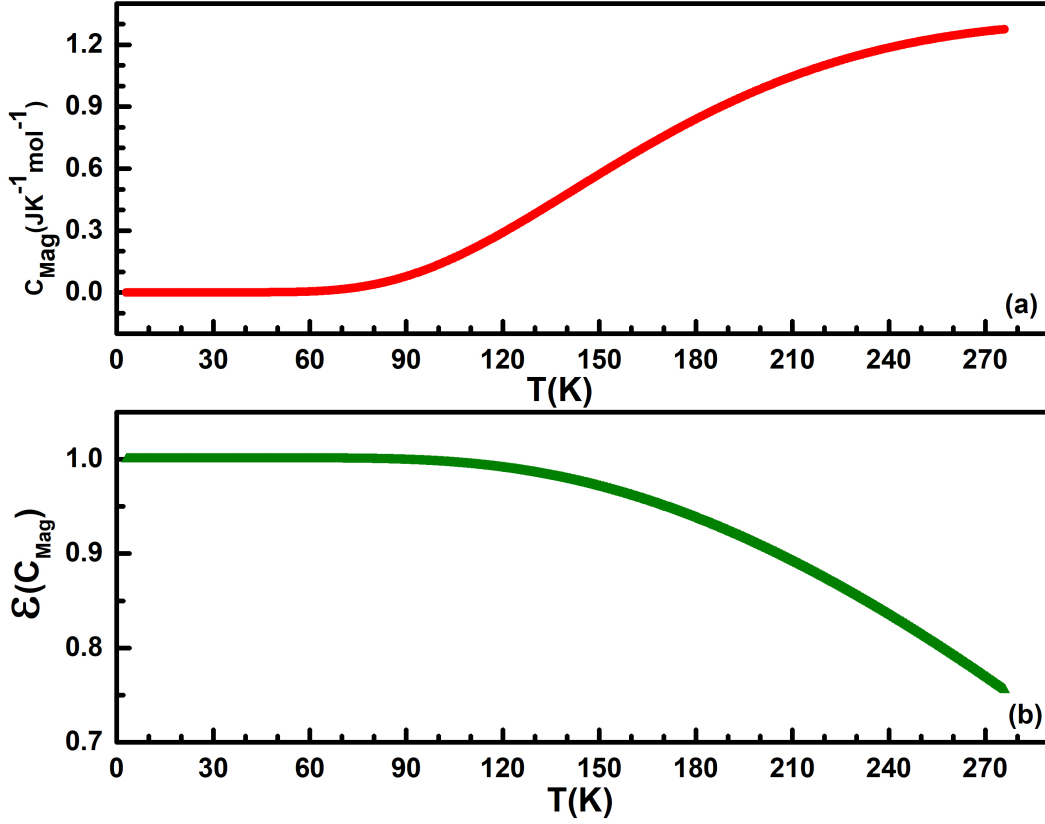


FIG. 9. (a) Temperature variation of magnetic contribution to specific heat, C_{Mag} , extracted from the fit to equation 30. (b) Temperature variation of distance between the states in terms of specific heat, $\mathcal{E}(C_{Mag})$, calculated using equation 26 using the extracted specific heat data in (a).

~ 260 K, in excellent agreement to the susceptibility data.

Temperature variation of distance between the states in terms of specific heat $\mathcal{E}(C_{Mag})$, can now be extracted from C_{Mag} obtained in Fig. 9 (a), using equation 26 and plotted in Fig. 9 (b). From the figure, it can be seen that $\mathcal{E}(C_{Mag})$ is maximum at 1 at the lowest measured temperature of 3 K and stays at 1 till a temperature of ~ 60 K. This behaviour is consistent with the temperature variation of $\mathcal{E}(\chi)$ (see Fig. 7 and discussions therein). Similar to the behaviour of $\mathcal{E}(\chi)$, $\mathcal{E}(C_{Mag})$ starts to decrease above 60 K due to the population of triplons across the energy gap. However, the decrease is a bit slower than $\mathcal{E}(\chi)$. But the two independent calculation shows that finite entanglement exists above room temperature.

VI. CONCLUSION

In conclusion, applying a theoretical measure termed as "distance between the states", we have quantified bipartite entanglement of a one dimensional magnetic dimer system via thermodynamical observables like susceptibility and specific heat. Experimental verification of bipartite entanglement was done on copper acetate which is a very well established magnetic dimer and consequently an excellent system to test the bipartite entanglement calculations. Large sized single crystals of copper acetate were grown by a slow evaporation technique and were characterised by techniques such as single crystal XRD, TGA, IR and Raman spectroscopy. In order to investigate the magnetic interactions, we conducted a comparative analysis with DFT computations using dual basis (B3LYP/6-311++G(d,p), B3LYP/LanL2DZ). Delocalisation index was then calculated for different bonds and shown that direct exchange between the copper atoms is not likely and the magnetic interactions occur via indirect superexchange. Temperature variation of both magnetic susceptibility as well as specific heat demonstrates the existence of bipartite entanglement till room temperature demonstrating the potential usefulness of this dimer system for quantum computations.

ACKNOWLEDGMENTS

D. J-N. acknowledges financial support from SERB, DST, Govt. of India (Grant No. CRG/2021/001262). Kakarlamudi Akhil Chakravarthy is acknowledged for his help in calculations during the initial stages of the work.

-
- [1] Xu, J., Assoud, A., Soheilnia, N., Derakhshan, S., Cuthbert, H.L., Greedan, J.E., Whangbo, M.H. and Kleinke, H., 2005. Synthesis, structure, and magnetic properties of the layered copper (II) oxide $\text{Na}_2\text{Cu}_2\text{TeO}_6$. *Inorganic chemistry*, 44(14), pp.5042-5046. DOI: <https://doi.org/10.1021/ic0502832>
 - [2] G. M. Pires, A., Quantum fluctuations in low-dimensional easy-plane spin models, *Eur. Phys. J. B* 44, 169–174 (2005), DOI: <https://doi.org/10.1140/epjb/e2005-00111-x>.
 - [3] Daoud, A. and Salah, A. Ben and Chappert, C. and Renard, J. P. and Cheikhrouhou, A. and Duc, Tranqui and Verdaguer, M.; (1986). Crystal structure and magnetic properties of

- piperazinium hexadichlorocuprate: A new $S=(1/2)$ antiferromagnetic chain with alternating exchange. , 6253–6260. DOI: <https://link.aps.org/doi/10.1103/PhysRevB.33.6253>
- [4] Infrared and Raman Spectra of Inorganic and Coordination Compounds. Part B: Application in Coordination, Organometallic, and Bioinorganic Chemistry, 5th Edition (Nakamoto, Kazuo) DOI: <https://doi.org/10.1021/ed077p1122.1>
- [5] Duffy, William; Barr, Kevin P. (1968). Theory of Alternating Antiferromagnetic Heisenberg Linear Chains. Physical Review, 165(2), 647–654. DOI: <https://doi.org/10.1103/PhysRev.165.647>
- [6] Bonner, J.C., Blöte, H.W.J., Bray, J.W. and Jacobs, I.S., 1979. Susceptibility calculations for alternating antiferromagnetic chains. Journal of Applied Physics, 50(B3), pp.1810-1812. DOI: <https://doi.org/10.1063/1.327177>
- [7] Landee, C.P. and Turnbull, M.M., 2014. A gentle introduction to magnetism: Units, fields, theory, and experiment. Journal of Coordination Chemistry, 67(3), pp.375-439. DOI: <https://doi.org/10.1080/00958972.2014.889294>
- [8] Aldoshin, S.M., Fel'dman, E.B. and Yurishchev, M.A., 2014. Quantum entanglement and quantum discord in magnetoactive materials. Low Temperature Physics, 40(1), pp.3-16. DOI: <https://doi.org/10.1063/1.4862469>
- [9] Bruker, S.M.A.R.T. and SAINT, X., 1997. Bruker Analytical X-ray Instruments Inc. Madison, WI, USA.
- [10] Bruker Analytical X-Ray Instruments Inc., 2015. SMART, SAINTPLUS V6. 02, SHELXTL V6. 10, and SADABS.
- [11] He, Z., Kyômen, T. and Itoh, M., 2004. $\text{BaCu}_2\text{V}_2\text{O}_8$: Quasi-one-dimensional alternating chain compound with a large spin gap. Physical Review B, 69(22), p.220407. DOI: <https://doi.org/10.1103/PhysRevB.69.220407>
- [12] Nawa, K., Michioka, C., Yoshimura, K., Matsuo, A. and Kindo, K., 2011. Magnetic phase diagram of alternating chain compound $\text{Pb}_2\text{V}_3\text{O}_9$. Journal of the Physical Society of Japan, 80(3), p.034710. DOI: [doi:10.1143/JPSJ.80.034710](https://doi.org/10.1143/JPSJ.80.034710)
- [13] Urushihara, D., Kawaguchi, S., Fukuda, K. and Asaka, T., 2020. Crystal structure and magnetism in the $S=1/2$ spin dimer compound $\text{NaCu}_2\text{VP}_2\text{O}_{10}$. IUCrJ, 7(4), pp.656-662. DOI: <https://doi.org/10.1107/S2052252520005655>

- [14] Yurishchev, M.A., 2011. Quantum discord in spin-cluster materials. *Physical Review B*, 84(2), p.024418. DOI:<https://link.aps.org/doi/10.1103/PhysRevB.84.024418>
- [15] Sahling, S., Remenyi, G., Paulsen, C., Monceau, P., Saligrama, V., Marin, C., Revcolevschi, A., Regnault, L.P., Raymond, S. and Lorenzo, J.E., 2015. Experimental realization of long-distance entanglement between spins in antiferromagnetic quantum spin chains. *Nature Physics*, 11(3), pp.255-260. DOI:<https://doi.org/10.1038/nphys3186>
- [16] Bose, S., 2003. Quantum communication through an unmodulated spin chain. *Physical review letters*, 91(20), p.207901. DOI: <https://link.aps.org/doi/10.1103/PhysRevLett.91.207901>
- [17] Apollaro, T.J., Almeida, G.M., Lorenzo, S., Ferraro, A. and Paganelli, S., 2019. Spin chains for two-qubit teleportation. *Physical Review A*, 100(5), p.052308. DOI: <https://link.aps.org/doi/10.1103/PhysRevA.100.052308>
- [18] Nikolopoulos, G.M. and Jex, I. eds., 2014. *Quantum state transfer and network engineering*. Springer Berlin Heidelberg.
- [19] Wootters, W.K., 1998. Entanglement of formation of an arbitrary state of two qubits. *Physical Review Letters*, 80(10), p.2245. DOI:<https://link.aps.org/doi/10.1103/PhysRevLett.80.2245>
- [20] O'connor, K.M. and Wootters, W.K., 2001. Entangled rings. *Physical Review A*, 63(5), p.052302. DOI: <https://link.aps.org/doi/10.1103/PhysRevA.63.052302>
- [21] Arnesen, M.C., Bose, S. and Vedral, V., 2001. Natural thermal and magnetic entanglement in the 1D Heisenberg model. *Physical Review Letters*, 87(1), p.017901. <https://link.aps.org/doi/10.1103/PhysRevLett.87.017901>
- [22] Wang, X. and Zanardi, P., 2002. Quantum entanglement and Bell inequalities in Heisenberg spin chains. *Physics Letters A*, 301(1-2), pp.1-6. DOI: <https://www.sciencedirect.com/science/article/pii/S037596010200885X>
- [23] Gu, S.J., Lin, H.Q. and Li, Y.Q., 2003. Entanglement, quantum phase transition, and scaling in the XXZ chain. *Physical Review A*, 68(4), p.042330. DOI: <https://link.aps.org/doi/10.1103/PhysRevA.68.042330>
- [24] Vedral, V., 2004. High-temperature macroscopic entanglement. *New Journal of Physics*, 6(1), p.102. DOI: <https://dx.doi.org/10.1088/1367-2630/6/1/102>
- [25] MarYááAtria, A. and TeresaáGarland, M., 1991. Magnetic properties of the alternating-chain compounds Cu (bipy)₂ (bipy= 2, 2-bipyridine, X= Br or Cl). *Journal of the Chemical Society, Dalton Transactions*, (10), pp.2707-2710. DOI:<http://dx.doi.org/10.1039/DT9910002707>

- [26] Ekert, A.K., 1991. Quantum cryptography based on Bell's theorem. *Physical review letters*, 67(6), p.661. DOI:<https://link.aps.org/doi/10.1103/PhysRevLett.67.661>
- [27] Zaitseva, N., Carman, L., Glenn, A., Newby, J., Faust, M., Hamel, S., Cherepy, N. and Payne, S., 2011. Application of solution techniques for rapid growth of organic crystals. *Journal of Crystal Growth*, 314(1), pp.163-170. DOI: [10.1016/j.jcrysgro.2010.10.139](https://doi.org/10.1016/j.jcrysgro.2010.10.139)
- [28] Gregson, A.K., Martin, R.L. and Mitra, S., 1971. The magnetic anisotropy and electronic structure of binuclear copper (II) acetate monohydrate. *Proceedings of the Royal Society of London. A. Mathematical and Physical Sciences*, 320(1543), pp.473-486. DOI: <http://www.jstor.org/stable/77892>
- [29] Deutsch, D. and Jozsa, R., 1992. Rapid solution of problems by quantum computation. *Proceedings of the Royal Society of London. Series A: Mathematical and Physical Sciences*, 439(1907), pp.553-558. DOI: <http://doi.org/10.1098/rspa.1992.0167>
- [30] Nielsen, M. and Chuang, I.L., 1999. *Quantum Computing*. unpublished notes. DOI: <https://10.1017/CBO9780511976667>
- [31] Hao, X. and Zhu, S., 2005. Entanglement teleportation through 1D Heisenberg chain. *Physics Letters A*, 338(3-5), pp.175-181. DOI: <https://doi.org/10.1016/j.physleta.2005.02.037>
- [32] Becke, A.D., 1988. Density-functional exchange-energy approximation with correct asymptotic behavior. *Physical review A*, 38(6), p.3098. DOI: <https://link.aps.org/doi/10.1103/PhysRevA.38.3098>
- [33] Lee, C., Yang, W. and Parr, R.G., 1988. Development of the Colle-Salvetti correlation-energy formula into a functional of the electron density. *Physical review B*, 37(2), p.785. DOI:<https://link.aps.org/doi/10.1103/PhysRevB.37.785>
- [34] Venuti, L.C., Boschi, C.D.E. and Roncaglia, M., 2007. Qubit teleportation and transfer across antiferromagnetic spin chains. *Physical Review Letters*, 99(6), p.060401. DOI: <https://link.aps.org/doi/10.1103/PhysRevLett.99.060401>
- [35] Amico, L., Fazio, R., Osterloh, A. and Vedral, V., 2008. Entanglement in many-body systems. *Reviews of modern physics*, 80(2), p.517. DOI:<https://link.aps.org/doi/10.1103/RevModPhys.80.517>
- [36] Gühne, O. and Tóth, G., 2009. Entanglement detection. *Physics Reports*, 474(1-6), pp.1-75. DOI:<https://doi.org/10.1016/j.physrep.2009.02.004>

- [37] Osborne, T.J. and Nielsen, M.A., 2002. Entanglement in a simple quantum phase transition. *Physical Review A*, 66(3), p.032110. DOI:<https://link.aps.org/doi/10.1103/PhysRevA.66.032110>
- [38] Sheldrick, G. M. (2015). SHELXT – Integrated space-group and crystal-structure determination. *Acta Cryst. A*71, 3–8. DOI: <https://doi.org/10.1107/S2053273314026370>
- [39] Sheldrick, G.M., 2008. A short history of SHELX. *Acta Crystallographica Section A: Foundations of Crystallography*, 64(1), pp.112-122. DOI: <https://doi.org/10.1107/S0108767307043930>
- [40] Mathew, G., Silva, S.L., Jain, A., Mohan, A., Adroja, D.T., Sakai, V.G., Tomy, C.V., Banerjee, A., Goreti, R., Singh, R. and Jaiswal-Nagar, D., 2020. Experimental realization of multipartite entanglement via quantum Fisher information in a uniform antiferromagnetic quantum spin chain. *Physical Review Research*, 2(4), p.043329. DOI:<https://link.aps.org/doi/10.1103/PhysRevResearch.2.043329>
- [41] Bleaney, B. and Bowers, K.D., 1952. Anomalous paramagnetism of copper acetate. *Proceedings of the Royal Society of London. Series A. Mathematical and Physical Sciences*, 214(1119), pp.451-465. DOI: <https://10.1098/rspa.1952.0181>
- [42] Brukner, Č., Vedral, V. and Zeilinger, A., 2006. Crucial role of quantum entanglement in bulk properties of solids. *Physical Review A*, 73(1), p.012110. DOI: <https://link.aps.org/doi/10.1103/PhysRevA.73.012110>
- [43] Mathew, G., Francis, S., Rajak, N.K., Praveen, S.G., Tomy, C.V. and Jaiswal-Nagar, D., 2021. A Simple Synthesis Method for Growing Single Crystals of a Copper Coordination Polymer [Cu (C2O4)(4-aminopyridine) 2 (H2O)]_n, and its Theoretical and Physical Properties Studies. *Crystal Research and Technology*, 56(2), p.2000124. DOI: <https://DOI:10.1002/crat.202000124>
- [44] Kumar, S., Sebastian, A., Athira, S., Singh, R., Kakarlamudi, A.C., Alex, A.P., Reddy, S. and Jaiswal-Nagar, D., 2022. One-dimensional magnetism in a facile spin 1/2 Heisenberg antiferromagnet with a low saturation field. *CrystEngComm*, 24(27), pp.4910-4920. <http://dx.doi.org/10.1039/D2CE00331G>
- [45] Abkari, A., Chaabane, I. and Guidara, K., 2016. DFT (B3LYP/LanL2DZ and B3LYP/6311G+ (d, p)) comparative vibrational spectroscopic analysis of organic-inorganic compound bis (4-acetylanilinium) tetrachlorocuprate (II). *Physica E: Low-dimensional Systems and Nanostructures*, 81, pp.136-144. DOI:<https://doi.org/10.1016/j.physe.2016.03.010>

- [46] Fernando, A., Weerawardene, K.D.M., Karimova, N.V. and Aikens, C.M., 2015. Quantum mechanical studies of large metal, metal oxide, and metal chalcogenide nanoparticles and clusters. *Chemical reviews*, 115(12), pp.6112-6216. DOI: <https://doi.org/10.1021/cr500506r>
- [47] Vedral, V., Plenio, M.B., Rippin, M.A. and Knight, P.L., 1997. Quantifying entanglement. *Physical Review Letters*, 78(12), p.2275. DOI: <https://link.aps.org/doi/10.1103/PhysRevLett.78.2275>
- [48] Koziskova J., Hahn F., Richter J. and Kožíšek J. (2016) Comparison of different absorption corrections on the model structure of tetrakis(μ -2-acetato)-diaqua-di-copper(II). *Acta Chimica Slovaca*, Vol.9 (Issue 2), pp. 136-140. DOI: <https://doi.org/10.1515/acs-2016-0023>
- [49] Witte, C. and Trucks, M., 1999. A new entanglement measure induced by the Hilbert–Schmidt norm. *Physics Letters A*, 257(1-2), pp.14-20. DOI: [https://doi.org/10.1016/S0375-9601\(99\)00279-0](https://doi.org/10.1016/S0375-9601(99)00279-0)
- [50] Cima, O.D., Franco, D.H.T. and da Silva, S.L.L., 2016. Quantum entanglement in trimer spin-1/2 Heisenberg chains with antiferromagnetic coupling. *Quantum Studies: Mathematics and Foundations*, 3, pp.57-63. DOI: <https://doi.org/10.1007/s40509-015-0059-1>
- [51] Johnston, D.C., Kremer, R.K., Troyer, M., Wang, X., Klümper, A., Bud'ko, S.L., Panchula, A.F. and Canfield, P.C., 2000. Thermodynamics of spin S= 1/2 antiferromagnetic uniform and alternating-exchange Heisenberg chains. *Physical Review B*, 61(14), p.9558. DOI: <https://doi.org/10.1103/PhysRevB.61.9558>
- [52] Lu, T. and Chen, F., 2012. Multiwfn: A multifunctional wavefunction analyzer. *Journal of computational chemistry*, 33(5), pp.580-592. <https://doi.org/10.1002/jcc.22885>
- [53] Bertolotti, F., Forni, A., Gervasio, G., Marabello, D. and Diana, E., 2012. Experimental and theoretical charge density of hydrated cupric acetate. *Polyhedron*, 42(1), pp.118-127. DOI: <https://doi.org/10.1016/j.poly.2012.05.005>
- [54] Kuz'mina, N.E., Palkina, K.K., Polyakova, N.V., Strashnova, S.B., Koval'chukova, O.V., Zaitsev, B.E. and Levov, A.N., 2001. Synthesis, Crystal Structure, and IR Absorption Spectra of the Adduct of Copper (II) Acetate Monohydrate with 1-Amino-4-aza-9-fluorenone $\text{Cu}_2(\text{CH}_3\text{COO})_4(\text{H}_2\text{O})_2 \cdot \text{C}_{12}\text{H}_8\text{N}_2\text{O}$. *Russian Journal of Coordination Chemistry*, 27, pp.711-716. DOI: <https://doi.org/10.1023/a:1012302325673>
- [55] Fradera, X., Austen, M.A. and Bader, R.F., 1999. The Lewis model and beyond. *The Journal of Physical Chemistry A*, 103(2), pp.304-314. DOI: <https://doi.org/10.1021/jp983362q>

- [56] Lu, T. and Chen, F., 2012. Multiwfn: A multifunctional wavefunction analyzer. *Journal of computational chemistry*, 33(5), pp.580-592. DOI:<https://doi.org/10.1002/jcc.22885>
- [57] Holladay, A., Leung, P. and Coppens, P., 1983. Generalized relations between d-orbital occupancies of transition-metal atoms and electron-density multipole population parameters from X-ray diffraction data. *Acta Crystallographica Section A: Foundations of Crystallography*, 39(3), pp.377-387. DOI:<https://doi.org/10.1107/S0108767383000823>
- [58] Koritsanszky, T.S. and Coppens, P., 2001. Chemical applications of X-ray charge-density analysis. *Chemical reviews*, 101(6), pp.1583-1628. DOI: <https://doi.org/10.1021/cr990112c>
- [59] Macchi, P. and Sironi, A., 2003. Chemical bonding in transition metal carbonyl clusters: complementary analysis of theoretical and experimental electron densities. *Coordination Chemistry Reviews*, 238, pp.383-412. DOI:[https://doi.org/10.1016/S0010-8545\(02\)00252-7](https://doi.org/10.1016/S0010-8545(02)00252-7)
- [60] Elango, M., Deepa, M., Subramanian, R. and Mohamed Musthafa, A., 2018. Synthesis, characterization, and antibacterial activity of polyindole/Ag-Cuo nanocomposites by reflux condensation method. *Polymer-Plastics Technology and Engineering*, 57(14), pp.1440-1451. DOI:<https://doi.org/10.1080/03602559.2017.1410832>
- [61] Narang, S.N., Kartha, V.B. and Patel, N.D., 1992. Fourier transform infrared spectra and normal vibrations of CuO. *Physica C: Superconductivity*, 204(1-2), pp.8-14. DOI:[https://doi.org/10.1016/0921-4534\(92\)90566-U](https://doi.org/10.1016/0921-4534(92)90566-U)
- [62] Mathey, Y., Greig, D.R. and Shriver, D.F., 1982. Variable-temperature Raman and infrared spectra of the copper acetate dimer $\text{Cu}_2(\text{O}_2\text{CCH}_3)_4(\text{H}_2\text{O})_2$ and its derivatives. *Inorganic Chemistry*, 21(9), pp.3409-3413. DOI:<https://doi.org/10.1021/ic00139a028>
- [63] Lin, Z., Han, D. and Li, S., 2012. Study on thermal decomposition of copper (II) acetate monohydrate in air. *Journal of thermal analysis and calorimetry*, 107(2), pp.471-475. DOI:<https://doi.org/10.1007/s10973-011-1454-4>
- [64] Youssef, I., Sall, S., Dintzer, T., Labidi, S. and Petit, C., 2019. Forward looking analysis approach to assess copper acetate thermal decomposition reaction mechanism. *American Journal of Analytical Chemistry*, 10(5), pp.153-170. DOI:<https://doi.org/10.4236/ajac.2019.105014>
- [65] He, Z., Kyômen, T. and Itoh, M., 2004. $\text{BaCu}_2\text{V}_2\text{O}_8$: Quasi-one-dimensional alternating chain compound with a large spin gap. *Physical Review B*, 69(22), p.220407. DOI:<https://link.aps.org/doi/10.1103/PhysRevB.69.220407>

- [66] Mookherji, A., 1963. Magnetic Studies on Cu^{++} Ion in Cupric Acetate Monohydrate Crystal. *Journal of the Physical Society of Japan*, 18(7), pp.977-980. DOI:<https://doi.org/10.1143/JPSJ.18.97>
- [67] Ghoshray, K., Pahari, B., Bandyopadhyay, B., Sarkar, R. and Ghoshray, A., 2005. V 51 NMR study of the quasi-one-dimensional alternating chain compound $\text{BaCu}_2\text{V}_2\text{O}_8$. *Physical Review B*, 71(21), p.214401. DOI:<https://link.aps.org/doi/10.1103/PhysRevB.71.214401>
- [68] Li, H., Yao, H., Zhang, E., Jia, Y., Hou, H. and Fan, Y., 2011. Crystal structures and magnetism of infinite alternating chains arranged by paddle-wheel dinuclear copper and mononuclear copper units. *Dalton Transactions*, 40(37), pp.9388-9393. DOI:<http://dx.doi.org/10.1039/C1DT10822K>
- [69] Frisch, M.E., Trucks, G.W., Schlegel, H.B., Scuseria, G.E., Robb, M.A., Cheeseman, J.R., Scalmani, G., Barone, V.P.G.A., Petersson, G.A., Nakatsuji, H.J.R.A. and Li, X., 2016. Gaussian 16.
- [70] Kundu, S., Shahee, A., Chakraborty, A., Ranjith, K.M., Koo, B., Sichelschmidt, J., Telling, M.T., Biswas, P.K., Baenitz, M., Dasgupta, I. and Pujari, S., 2020. Gapless Quantum Spin Liquid in the Triangular System $\text{Sr}_3\text{CuSb}_2\text{O}_9$. *Physical Review Letters*, 125(26), p.267202. DOI:<https://link.aps.org/doi/10.1103/PhysRevLett.125.267202>
- [71] Gopal, E., 2012. Specific heats at low temperatures. Springer Science and Business Media. DOI:<https://books.google.co.in/books?id=KrE3yQEACAAJ>
- [72] Eremina, R.M., Gavrilova, T.P., Günther, A., Wang, Z., Lortz, R., Johnsson, M., Berger, H., Krug von Nidda, H.A., Deisenhofer, J. and Loidl, A., 2011. Magnetization and specific heat of the dimer system CuTe_2O_5 . *The European Physical Journal B*, 84, pp.391-395. DOI:<https://doi.org/10.1140/epjb/e2011-20263-2>
- [73] Joshua, S.J., 1998. Magnon contribution to the specific heat and the validity of power laws in antiferromagnetic crystals. *Physica A: Statistical Mechanics and its Applications*, 261(1-2), pp.135-142. DOI:[https://doi.org/10.1016/s0378-4371\(98\)00370-7](https://doi.org/10.1016/s0378-4371(98)00370-7)
- [74] Tari, A. ed., 2003. The specific heat of matter at low temperatures. World Scientific. DOI:<https://www.worldscientific.com/doi/abs/10.1142/p254>
- [75] Nawa, K., Michioka, C., Yoshimura, K., Matsuo, A. and Kindo, K., 2012, March. Single crystal growth and magnetic property of $\text{NH}_4\text{CuPO}_4 \cdot \text{H}_2\text{O}$. In *Journal of Physics: Conference Series* (Vol. 344, No. 1, p. 012024). IOP Publishing. DOI:<https://doi.org/10.1088/1742->

6596/344/1/012024

- [76] Johnston, D. C.; Kremer, R. K.; Troyer, M.; Wang, X.; Klümper, A.; Bud'ko, S. L.; Panchula, A. F.; Canfield, P. C. (2000). antiferromagnetic uniform and alternating-exchange Heisenberg chains. *Physical Review B*, 61(14), 9558–9606. DOI: <https://doi.org/10.1103/PhysRevB.61.9558>
- [77] Daoud, A.; Salah, A. Ben; Chappert, C.; Renard, J. P.; Cheikhrouhou, A.; Duc, Tran-qui; Verdaguer, M. (1986). Crystal structure and magnetic properties of piperazinium hexadichlorocuprate: A new $S=(1/2)$ antiferromagnetic chain with alternating exchange. *Physical Review B*, 33(9), 6253–6260. DOI: <https://doi.org/10.1103/PhysRevB.33.6253>
- [78] *Infrared and Raman Spectra of Inorganic and Coordination Compounds. Part A: Theory and Applications in Inorganic Chemistry*, 5th Edition (Nakamoto, Kazuo) DOI: <https://doi.org/10.1021/ed077p1122.1>
- [79] Piotr Drożdżewski; Anna Brożyna (2005). Metal isotope and density functional study of the tetracarboxylatodicopper(II) core vibrations. , 62(1-3), 703–710. DOI: <https://doi.org/10.1016/j.saa.2005.02.038>